Development of Predictive Models of the Kinetics of a Hydrogen Abstraction Reaction Combining Quantum-Mechanical Calculations and Experimental Data

Aikaterini Diamanti,[†] Claire S. Adjiman,[†] Patrick M. Piccione,[‡] Anita M. Rea,[¶] and Amparo Galindo[*,†]

Centre for Process Systems Engineering, Department of Chemical Engineering, Imperial College London, London, SW7 2AZ, UK, Process Studies Group, Technology and Engineering, Syngenta, Breitenloh 5, 4333 Münchwilen, Switzerland, and Process Studies Group, Technology and Engineering, Syngenta, Jealotts Hill International Research Center, Bracknell, Berkshire, RG42 6EY, United Kingdom

E-mail: a.galindo@imperial.ac.uk

Abstract

The importance of developing accurate modelling tools for the prediction of reaction kinetics is well recognised. In this work, a thorough investigation of the suitability of quantum mechanical (QM) calculations to predict the effect of temperature on the rate

[*]To whom correspondence should be addressed

[†]Centre for Process Systems Engineering, Department of Chemical Engineering, Imperial College London, London, SW7 2AZ, UK

[‡]Process Studies Group, Technology and Engineering, Syngenta, Breitenloh 5, 4333 Münchwilen, Switzerland

[¶]Process Studies Group, Technology and Engineering, Syngenta, Jealotts Hill International Research Center, Bracknell, Berkshire, RG42 6EY, United Kingdom

constant of the reaction between ethane and hydroxyl radical is presented. Further, hybrid models that combine a limited number of QM calculations and experimental data are developed in order to increase the model reliability. The activation energy barrier of the reaction is computed using various computational methods, such as B3LYP, M05-2X, M06-2X, MP2 and PMP2, CBS-QB3 and W1BD, with a selection of basis sets. A broad range of values is obtained, including negative barriers for all of the calculations with B3LYP. The rate constants are also obtained for each method, using conventional transition state theory, and are compared with available experimental values at 298 K. The best agreement is achieved with the M05-2X functional with cc-pV5Z basis set. Rate constants calculated at this level of theory are also found to be in good agreement with experimental values at different temperatures, resulting in a mean absolute error of the logarithm (MAE_{ln}) of the calculated values of 0.213 over a temperature range of 200-1250 K and 0.108 over a temperature range of 300-499 K. Tunnelling and vibrational anharmonicities are identified as important sources of discrepancies at low and high temperatures, respectively. Hybrid models are proposed and found to provide good correlated rate-constant values and to be competitive with conventional kinetic models, i.e., the Arrhenius and the three-parameter Arrhenius models. This combination of QM-calculated and experimental data sources is proved particularly beneficial when fitting to scarce experimental data. In this case, the model built on the hybrid strategy has parameters with significantly reduced uncertainty (reflected in the much narrower 95% confidence intervals) compared with the conventional kinetic models while also capturing well the experimental reaction rates with a MAE_{ln} of the rate constant of 0.118. This provides a useful strategy for kinetic model development.

Introduction

Understanding and modelling reaction kinetics are integral parts of process development. In areas such as combustion[1] and atmospheric chemistry[2] hydrogen abstraction reactions between hydroxyl radical and hydrocarbons are of specific interest. The modelling of chemical

kinetics in these areas requires the specification of a large number of rate constants over broad temperature ranges. In addition to their technological and scientific importance, hydrogen abstraction reactions have a simple mechanism that allows for detailed studies, and hence this class of reactions is very well-documented.[3,4]

Reliable sources of data may be found in databases reviewing experimental studies for the gas-phase rate constants for the reactions of hydroxyl radical with alkanes and cycloalkanes spanning temperature ranges from approximately 180 to 2000 K.[5–11] It is common practice to fit the experimental values to an empirical model, usually the Arrhenius equation,[12] to obtain kinetic parameters. The Arrhenius model contains two parameters: the pre-exponential factor and the activation energy, which are strictly applicable within the temperature interval used in the fitting. According to the Arrhenius equation, the logarithm of a reaction's rate constant is expected to be linear in the absolute inverse temperature. In kinetic studies where the rate constant is measured over a narrow temperature range (less than 100 K), this condition is usually verified. If the measured rate constants do not follow linearity, then one usually resorts to an expanded version of the Arrhenius equation[13] that includes one extra parameter to fit the data. (The reader is referred to reference (14) for a detailed review.)

Experimentally-deduced parameters in such empirical models are subject to uncertainty arising from measurement errors as well as limitations of the models. These limitations concern mainly empirical aspects, such as the nature of some formulas to be more linear than others (e.g., logarithmic plots tend to be more linear) and the number of parameters involved in the equations. Increasing the number of parameters usually results in a better fit to the experimental data, for example in the case of the generalized version of the Arrhenius equation; yet the quality of fit is not a sufficient argument for selecting a certain model over another and parametric uncertainty and predictive capabilities, as well as interpretability, must also be taken into account. The Arrhenius equation is a characteristic example of an empirical model that has historically prevailed over models with similar, or even better, fitting agreement because it contains parameters (e.g. the activation energy) that are mean-

ingfully linked to the occurring chemical reaction. However, empirical models cannot be used to determine all chemical phenomena occurring during a reaction. For example, particularly for the class of hydrogen abstraction reactions, phenomena such as tunnelling or the strong temperature-dependence of vibrational partition functions in the presence of low-frequency bending modes[15] are not captured by any empirical parameter.

Quantum-mechanical (QM) methods provide a promising alternative and may in principle be used to determine kinetic quantities such as rate constants, tunnelling and the temperature variation of partition functions. Since they do not depend on experimental data and may in theory provide a physically meaningful analysis of the kinetics, they are frequently used to undertake systematic kinetic studies of reacting systems. A number of comprehensive benchmark computational studies exists, in which the electronic activation barrier for diverse reaction types is calculated.[16,17] The activation barrier value is theoretically linked to the activation energy parameter of the Arrhenius equation.[18] In general, QM methods are computationally demanding, thus their use in large-scale engineering applications, such as for example in drug design where large biomolecules are of interest or furnace design where thousands of reactions take place, is prohibitive. Nevertheless, their use in small-size molecular systems of a few tens of atoms is affordable.

For the hydrogen abstraction reactions between the hydroxyl radical and alkanes, a number of computational studies has been presented in the literature[19–30] ranging from the basic framework of Hartree-Fock (HF) theory to very expensive compound methods, such as the popular G2 method,[31] and the coupled-cluster method with triple-excitation terms, CCSD(T).[32,33] Despite the large variety of computational methods tested, there is no clear consensus on which one is the most appropriate method to study the energetics for this class of reactions, as contradictory examples of their performance may be found. For example, the HF methods have been known to overestimate barrier heights due to the dynamical electron correlation energy change as the reaction proceeds from the reactants to the transition state.[34] Pure density functional theory (DFT) methods tend to underestimate the energy

barrier due to self-interaction errors which are prominent for non-equilibrium structures (such as transition states).[35–37] However, hybrid DFT methods, in which the exact HF exchange energy term varies, may appear to perform better for the computation of activation barriers due to significant error cancellations.[37,38] Compound methods, such as G2 or CBS-QB3, occasionally encounter performance issues due to problems with the ground-state zero-order HF description and possibly due to differences in the transition state geometry, which is usually computed at lower level of theory than the transition state energy.[39] In conjunction to the choice of method, the size and complexity of the basis set have a significant impact on the calculated activation energy value. As a result, the accuracy that may be expected from different QM levels of theory is open to critical evaluation, and hence, finding a universal level of theory that captures best the energetics of hydrogen abstraction reactions remains a challenge.

Here we present a systematic study of the reaction between ethane and hydroxyl radical

$$C_2H_6 + \cdot OH \rightleftharpoons [C_2H_5...H...OH]^{\ddagger} \rightarrow \cdot C_2H_5 + H_2O, \qquad \text{Scheme 1}$$

with a detailed investigation of temperature effects and the development of hybrid QM correlative models. We first calculate QM values for the activation energy barrier and the corresponding rate constant of this reaction using different levels of theory. Kinetic calculations are performed using conventional transition state theory (CTST)[40,41] with the Wigner tunnelling correction factor.[42] We then identify the level of theory that provides the most accurate value of the reaction rate constant at 298 K by comparison to experimental data and we report structural parameters and frequencies for the optimized structures. We find the hybrid DFT functional M05-2X with the cc-pV5Z basis set to be the most accurate level of theory, and proceed to use it to calculate reaction rates over a range of temperatures, from 200 to 1250 K. In the second part of this work we investigate the development of hybrid kinetic models that combine a small number of experimental reaction rate data with

QM-calculated activation energy values and reaction rate constants to estimate the parameters of the Arrhenius equation and its generalized version. Such correlative expressions may be used in large-scale process modelling due to their low computational cost. The level of accuracy to which we obtain parameters for the Arrhenius equation and its generalized version determines the predictive capability of the kinetic models derived. We therefore focus on identifying reliable modelling strategies for the prediction of reaction rate constants over broad temperature ranges based on accurately determined kinetic parameters for Scheme 1.

Computational details

QM calculations

All electronic structure calculations are performed using the software Gaussian 09 (release C.01).[43] Various levels of theory are considered for the calculation of the activation energy barrier of the reaction. In particular, the DFT functionals B3LYP,[44–47] M05-2X[48] and M06-2X,[49] the second-order Møller-Plesset perturbation theory MP2[50] and the equivalent spin projection method PMP2[51,52] are selectively combined with the following basis sets: 3-21G, 6-21G, 6-31G, 6-31G(d), 6-31G(d,p), 6-31+G(d,p), 6-311++G(d,p), 6-311G(2d,d,p), 6-311+G(2d,p), cc-pVTZ, aug-cc-pVTZ, cc-pVQZ, aug-cc-pVQZ, cc-pV5Z and CBSB7. In addition, the composite methods CBS-QB3[53,54] and W1BD[55,56] are considered; no basis set specification is required in these cases. The adj2-cc-pVTZ basis set, first adjusted by Melissas and Truhlar[19] to data for the reaction of interest, is also tested with the MP2 and PMP2 theories in the present work. All vibrational modes are calculated under the harmonic approximation. For B3LYP and MP2, the vibrational frequencies as well as the zero-point energies are scaled, by factors 0.9614 and 0.9427 respectively, to compensate for the inaccuracy of the functionals.[57]

Special techniques are available to describe systems involving radicals with unpaired spin electrons. Either an unrestricted approach or a restricted open-shell approach is usually

followed (for an example, see reference (58)), depending on whether electrons of opposite spin are allowed or not to occupy different spatial orbitals. The unrestricted approach gives values greater than 0.75 for the total spin-squared operator $<S^2>$, although 0.75 is the default value for a doublet state, due to spin contamination from higher energy states. The method allows however for more variational freedom, as the spatial restriction of opposite spin-electrons is removed, and as a result it leads to lower total energies. Lower energies are usually an indication of more stable conformations for a given molecular structure, but in this case this lowering may correspond to a more stable configuration or may be an artifact created by the unrestricted approach. On the other hand, the restricted open-shell approach results in a spin-contamination-free wave function and reasonable total energies; however, the singly occupied orbitals are not uniquely defined and the associated energies do not strictly obey Koopmans' theorem,[59] and are hence subject to physical misinterpretation. Additional schemes are also available for "projecting out" or "annihilating" the contaminant part of the unrestricted approach once the wave function has been obtained.[60] This comes at the price of an increase in the CPU time requirements.

Previous studies of reactions involving radicals have emphasized the need to take into account spin contamination for the accurate estimation of the activation energy barrier.[19,23–26,61] In our calculations, we adopt the unrestricted approach and the spin-projection approach. The value of $<S^2>$ is monitored to ensure the impact of spin contamination is minimal. The acceptable range is indicated by the empirical rule, presented by Young,[62] according to which the effect of spin contamination is not significant if there is less than 10% difference between the values of $<S^2>$ and S(S+1).

Rate-constant calculations

Considering a bimolecular gas-phase reaction, given as

$$\nu_{\mathrm{A}}\mathrm{A} + \nu_{\mathrm{B}}\mathrm{B} \overset{K_c^{\ddagger}}{\rightleftharpoons} \nu_{\mathrm{AB}^{\ddagger}}\mathrm{AB}^{\ddagger} \xrightarrow{k^{\ddagger}} \text{products}, \qquad \text{Scheme 2}$$

the ideal-gas reaction rate constant k^{IG} may be computed using conventional transition state theory[40,41,63] (CTST) following

$$k^{\mathrm{IG}} = \kappa \frac{k_{\mathrm{B}} T}{h} \prod_{i=\mathrm{A,B,AB}^{\ddagger}} \left(\frac{RT}{p^{\circ}} \right)^{-\nu_i} \exp\left(-\frac{\Delta^{\ddagger} \underline{G}^{\circ,\mathrm{IG}}}{RT} \right), \tag{1}$$

where κ is the transmission coefficient to correct for tunnelling effects, k_{B} the Boltzmann constant, T the absolute temperature, h the Planck constant, R the ideal gas constant, p° the standard-state pressure (1 atm) and ν_i the stoichiometric coefficient of species i for $i = \mathrm{A}, \mathrm{B}$ (reactants) and $\mathrm{AB}^{\ddagger}$ (transition state) for Scheme 2. $\underline{G}^{\circ,\mathrm{IG}}$ is the ideal-gas molar Gibbs free energy and $\Delta^{\ddagger}$ stands for the difference between the transition state and the reactants, weighted by the values of the stoichiometric coefficients, so that

$$\Delta^{\ddagger} \underline{G}^{\circ,\mathrm{IG}} = \nu_{\mathrm{AB}^{\ddagger}} \underline{G}^{\circ,\mathrm{IG}}_{\mathrm{AB}^{\ddagger}} + \nu_{\mathrm{A}} \underline{G}^{\circ,\mathrm{IG}}_{\mathrm{A}} + \nu_{\mathrm{B}} \underline{G}^{\circ,\mathrm{IG}}_{\mathrm{B}}, \tag{2}$$

where in Scheme 2 ν_{A} and ν_{B} are negative.

Equation (1) may also be formulated in terms of the corresponding partition functions of the different species as

$$k^{\mathrm{IG}} = \kappa \frac{k_{\mathrm{B}} T}{h} \prod_{i=\mathrm{A,B,AB}^{\ddagger}} \left(\frac{RT}{p^{\circ}} \right)^{-\nu_i} \prod_{i=\mathrm{A,B,AB}^{\ddagger}} \left(q_i^{\prime,\mathrm{IG}}(T) \right)^{\nu_i} \exp\left(-\frac{\Delta^{\ddagger} \underline{E}^{\mathrm{el,IG}}}{RT} \right), \tag{3}$$

where the ideal-gas molar Gibbs free energy term has been replaced by the product of the ideal-gas molecular partition function of each species i at temperature T, $q_i^{\prime,\mathrm{IG}}(T)$, and the ideal-gas electronic energy $\underline{E}^{\mathrm{el,IG}}$.[64]

Tunnelling effects may be described quantitatively following one-dimensional methods such as those of Wigner,[42] Skodje and Truhlar[65] and Eckart,[66] where the reaction path and the tunnelling path coincide. These approaches result in simple analytic expressions for the transmission coefficient and this makes them attractive in kinetic applications because of

their low computational cost. Here we use the Wigner correction factor[42]

$$\kappa = 1 + \frac{1}{24}\left(\frac{h\nu^{\ddagger}}{k_{\mathrm{B}}T}\right)^{2}, \tag{4}$$

where $\nu^{\ddagger}$ is the magnitude of the imaginary frequency of the transition state structure in cm^{-1}. In general, Wigner's approach predicts a larger tunnelling effect for reactions having thin barriers (large $\nu^{\ddagger}$) than wide barriers (small $\nu^{\ddagger}$).[15] In hydrogen-transfer reactions tunnelling may be important;[39,67–69] in this study the effectiveness of the Wigner expression is assessed. Although more advanced methods have been developed to address tunnelling, i.e. small curvature tunnelling[70,71] (SCT) or large curvature tunnelling[72] (LCT) methods, these are not considered here.

Computational investigation of the reaction kinetics

Activation energy barrier

The value for the activation energy at 298 K for Scheme 1 has been reported by Atkinson[10] as 9.11 kJ mol^{-1} (uncertainty range 8.99-9.22 kJ mol^{-1}) deduced from experimental kinetic data. Our calculated electronic activation energy barriers at 0 K, including the zero-point vibrational energy corrections, for 37 selected combinations of methods and basis sets (levels of theory) are presented in Table 1.

As may be seen in Table 1, a broad range of values is obtained, including negative values for the case of the B3LYP family of functionals. Negative values for the electronic activation energy barrier of Scheme 1 were also reported by Hu et al.,[30] who find a value of -4.18 kJ mol^{-1}, close to the one reported here (-4.01 kJ mol^{-1}), using B3LYP/6-311++G(d,p). Kobayashi et al.[61] reported a negative barrier height of -13.4 kJ mol^{-1} using B3LYP/cc-pVTZ for Scheme 1. Hybrid DFT methods have been noted to underestimate systematically the barrier heights of hydrogen abstraction reactions[20,73–76] (sometimes by tens of kJ mol^{-1}).

In particular, relating to B3LYP, Chandra and Uchimaru[77] have suggested this method is unreliable for calculations of this class of reactions. Lynch and Truhlar[38] investigated a test set of 22 reactions (including Scheme 1) and concluded that B3LYP is one of the least effective electronic structure methods for determining barrier heights. Through careful examination of DFT methods it has been suggested that the Hartree-Fock exchange part of the calculation is responsible for this discrepancy.[78] An empirical localized orbital correction model has been proposed by Hall et al.[79] to redress this shortcoming of DFT methods. When applied to the B3LYP functional particularly, this empirical scheme resulted in a mean unsigned error value reduced by 8 kJ mol^{-1} compared with the uncorrected B3LYP calculations for a large dataset of 105 barriers heights.

The M05-2X and M06-2X functionals give positive activation barriers, which is encouraging, although it may also be appreciated from the table that a broad range of values is obtained for different basis sets. For the family of basis sets developed by Ditchfield et al.,[88] the value of the electronic activation energy barrier found using the modest 6-31G(d) basis set is 15.26 kJ mol^{-1}. As we augment this basis set by adding polarization and diffuse functions the value of the electronic activation energy barrier decreases to 8.69 kJ mol^{-1} for M05-2X with the 6-311+G(2d,p) basis set and to 9.32 kJ mol^{-1} for M06-2X with the 6-311++G(d,p) basis set. By using Dunning's[89,90] correlation-consistent basis sets (cc-pVTZ, cc-pVQZ, cc-pV5Z) and their augmented (aug-) forms with diffuse functions, the lowering of the reaction barrier height is even more pronounced. Particularly for M05-2X we generate activation barriers that are amongst the lowest positive values computed in our work, ranging from the lowest overall value found with cc-pV5Z at 6.65 kJ mol^{-1} up to 7.12 kJ mol^{-1} with cc-pVQZ basis set. We also test the CBSB7[53] basis set which constitutes one of the multiple steps of the CBS-QB3 method. For M05-2X and M06-2X with this basis set the values of the activation barrier are 8.79 kJ mol^{-1} and 8.29 kJ mol^{-1}, respectively.

Scheme 1 has been included in the HTBH38/4 database[16,91] as part of the test set for assessing the performance of the M05-2X and M06-2X functionals from Zhao et al.[48,49]

Table 1: Electronic activation energy barriers $\Delta^{\ddagger}\underline{E}^{\mathrm{el,IG}}$, corrected for the zero-point vibrational energy, calculated for various electronic structure QM methods. Rate constants k^{IG} are calculated using CTST (Equation (3)) at 298 K and compared with available experimental values $k^{\mathrm{Expt.}}$ at 298 K from the literature. The uncertainty for the experimental values $k^{\mathrm{Expt.}}$ at 298 K is given within the parenthesis.

	$\Delta^{\ddagger}\underline{E}^{\mathrm{el,IG}}$/kJ mol^{-1}			k^{IG} $\times 10^{-8}$/dm^3 mol^{-1} s^{-1}
Level of theory	This work	Previous studies	Ref.	This work
B3LYP/3-21G	−9.84			1661
B3LYP/6-21G	−3.18			118.9
B3LYP/6-31G	−2.04			56.53
B3LYP/6-31G(d)	−2.01			60.71
B3LYP/6-31+G(d,p)	−4.35			185.2
B3LYP/6-311++G(d,p)	−4.01	-4.18	[30]	74.53
B3LYP/6-311G(2d,d,p)	−6.03			179.5
M05-2X/6-31G(d)	15.26			0.0706
M05-2X/6-31+G(d,p)	9.02			0.4140
M05-2X/6-311++G(d,p)	9.23			0.3601
M05-2X/6-311+G(2d,p)	8.69			0.4775
M05-2X/CBSB7	8.79			0.3855
M05-2X/aug-cc-pVTZ	6.82			1.133
M05-2X/cc-pVQZ	7.12			0.9734
M05-2X/aug-cc-pVQZ	6.98			1.094
M05-2X/cc-pV5Z	6.65			1.556
M06-2X/6-31G(d)	13.27			0.1817
M06-2X/6-31+G(d,p)	9.01			0.3870
M06-2X/6-311++G(d,p)	9.32			0.2463
M06-2X/CBSB7	8.29			0.4685
M06-2X/aug-cc-pVTZ	7.91			0.7162
MP2/6-31G(d)	39.46			0.000008127
MP2/6-31+G(d,p)	27.74			0.0005691
MP2/6-311++G(d,p)	25.04	25.53	[30]	0.001290
MP2/6-311+G(2d,p)	23.54	5.76[a]/22.33[b]	[21]	0.002588
MP2/cc-pVTZ	20.50	17.20[c]	[27]	0.01163
MP2/adj2-cc-pVTZ	19.98	17.33	[19]	0.01827
MP2/cc-pVQZ	19.10			0.01978
PMP2/6-31G(d)	29.59			0.0004355
PMP2/6-31+G(d,p)	19.91			0.01337
PMP2/6-311++G(d,p)	17.06	17.53	[30]	0.03221
PMP2/6-311+G(2d,p)	15.87	-8.00[a]/13.06[b]	[21]	0.05705
PMP2/cc-pVTZ	12.80			0.2597
PMP2/adj2-cc-pVTZ	12.30	9.75[d]	[19]	0.4048
PMP2/cc-pVQZ	11.81			0.3732
CBS-QB3	9.45			0.3202
W1BD	11.49			0.1492

Experimental studies	$k^{\mathrm{Expt.}}$ $\times 10^{-8}$/dm^3 mol^{-1} s^{-1}	Ref.
Greiner (1970)	2.048 (0.060)	[80]
Leu (1979)	1.566 (0.241)	[81]
Jeong et al. (1984)	1.843 (0.126)	[82]
Schiffman et al. (1991)	1.463 (0.072)	[83]
Dóbé et al. (1991,1992)	1.650 (0.241)	[84,85]
Sharkey and Smith (1993)	1.777 (0.084)	[86]
Finlayson-Pitts et al. (1993)	1.662 (0.042)	[87]
	1.626 (0.070)	[87]
Atkinson (2003)[e]	1.496 (0.300)	[10]

[a] Single-point energy calculation for geometries optimized at the HF/6-31G(d,p) level of theory.
[b] Single-point energy calculation for geometries optimized at the MP2/6-31G(d,p) level of theory
[c] Optimized at the MP2/aug-cc-pVDZ level of theory.
[d] Single-point energy calculation for geometries optimized at the MP2/adj2-cc-pVTZ level of theory.
[e] Recommended expression based on experimental data, evaluated at 298 K.

In this database the value reported for the barrier height of Scheme 1 is 14.2 kJ mol^{-1}. Comparing this value with single-point energy calculations performed with the MG3S basis set gives a mean unsigned error (MUE) of 5.61 kJ mol^{-1} for the M05-2X functional and of 4.73 kJ mol^{-1} for the M06-2X functional. To the best of our knowledge, Scheme 1 has not been studied elsewhere using the M05-2X and M06-2X functionals, despite the existence of several studies that have highlighted the suitability of these functionals for the computation of barrier heights and their broad applicability to similar chemical systems.[48,75,92]

The performance of the MP2 and PMP2 methods is tested using the same selection of basis sets. The choice of basis set is found to alter the energy barrier significantly: as expected, the more extensive the basis set used, the lower the barrier height obtained. For example, when the relatively small 6-31G(d) basis set is used, the activation energy barrier is calculated to be 39.46 kJ mol^{-1}. The value decreases by half when using the much more extensive cc-pVQZ basis set, resulting in a value of 19.10 kJ mol^{-1}. Similarly for the PMP2 method, the energy found decreases from 29.59 kJ mol^{-1} for the 6-31G basis set to 11.81 kJ mol^{-1} for the cc-pVQZ basis set. In comparison with MP2, the barrier heights calculated with PMP2 are on average 8.00 kJ mol^{-1} lower. This difference may be ascribed to the use of the projected method to treat spin-contamination effects embedded in PMP2. The spin-contamination treatment of the projected method is distinctly reflected in the value of the activation barrier. Several studies may be found in the literature in which MP2 or PMP2 methods are used for calculating the energetics of Scheme 1. Sekusak et al.[21] report a single-point energy value at the MP2/6-311+G(2d,p) level of theory (with the geometries optimized at the HF/6-31G(d,p) level of theory) of 5.76 kJ mol^{-1} and a single-point energy value at the PMP2/6-311+G(2d,p) level of theory (with the geometries optimized at the HF/6-31G(d,p) level of theory) of -8.00 kJ mol^{-1}. In the same study, when optimizing the geometries at the MP2/6-31G(d,p) level of theory the corresponding energy values reported are significantly different: 22.33 kJ mol^{-1} for a single-point energy calculation at the MP2/6-311+G(2d,p) level of theory and 13.06 kJ mol^{-1} for a single-point energy calculation at the

PMP2/6-311+G(2d,p) level of theory. For more complex basis sets Hashimoto and Iwata[27] performed calculations at the MP2/aug-cc-pVDZ level of theory resulting in an activation energy barrier of 17.20 kJ mol^{-1}. Our value using the cc-pVTZ basis set devoid of diffuse functions at the MP2 level is 20.50 kJ mol^{-1}. An interesting basis set, employed here in conjunction with the MP2 and PMP2 methods, is the adj2-cc-pVTZ, basis set created by Melissas and Truhlar[19] using Gaussian 92. It has a modified f-shell function for the oxygen atom, in order to equate the scaling factors of the formation of the O−H bond and the breaking of the C−H bond occurring during Scheme 1. We reproduce this basis set following the same modification procedure. For the MP2 and the PMP2 methods our values of 19.98 kJ mol^{-1} and 12.30 kJ mol^{-1}, respectively, are on average 2.60 kJ mol^{-1} higher than their single-point energy values (17.33 kJ mol^{-1} and 9.75 kJ mol^{-1}, respectively). The change of version of the software package used may reasonably explain these energy variations.

The composite CBS-QB3 and W1BD methods are also evaluated here. These are computational methods which include a number of pre-defined QM calculations and they are expected to be highly reliable. Usually, one achieves a good description of reaction energetics using these methods and although they are computationally more demanding than DFT and MP2 methods, the small molecules treated here render them affordable to use. We compute barrier heights of 9.45 kJ mol^{-1} for CBS-QB3 and 11.49 kJ mol^{-1} for W1BD. These values are lower than any of those found with the MP2 and PMP2 levels of theory and than those found with M05-2X and M06-2X levels of theory together with the 6-31G(d) basis set. The value of 9.45 kJ mol^{-1} obtained with CBS-QB3 is in good agreement with the values calculated with M05-2X/6-311++G(d,p) (9.23 kJ mol^{-1}) and with M06-2X/6-311++G(d,p) (9.32 kJ mol^{-1}). The slightly higher value of 11.49 kJ mol^{-1} with W1BD agrees best with the values derived from PMP2/cc-pVQZ (11.81 kJ mol^{-1}) and from PMP2/adj2-cc-pVTZ (12.30 kJ mol^{-1}).

As may be appreciated by inspecting Table 1, the range of values for the energetics obtained from the different electronic-structure methods is remarkably broad. The values

for the activation energy barrier cover a range of almost 50 kJ mol^{-1} (including negative values). Some general trends are also noticeable in our calculations, in particular, lower values of activation energy barriers are obtained with larger basis sets and with a better treatment of spin contamination. The activation energy barrier is the determining factor in the calculation of the rate constant (cf. Equation (3)), and hence this broad variability concomitantly leads to rate constant values spanning over eight orders of magnitude. This large variation may be rationalized on the basis of the approximations and assumptions attributed to each computational method as well as the size of the basis set used in any case. The combination of the method and basis set dramatically influences the electronic energy barrier values.

Reaction rate constant at 298 K

The rate constant value for Scheme 1 at 298 K recommended by Atkinson[10] is as 1.496×10^{8} dm^3 mol^{-1} s^{-1}. This value is derived from the evaluation of a three-parameter Arrhenius-type expression fitted to a large number of experimental data points over a temperature range from 180 to 1230 K.

Using our calculated activation barriers, the rate constant of Scheme 1 at 298 K is computed using CTST (Equation (3)) for each of the levels of theory presented. The values are given in Table 1 and plotted in Figure 1.

The exponential term in the CTST expression plays a dominant role in determining the rate constant value. Therefore, as expected given the calculated barrier heights, the rate of the reaction is considerably overestimated with the B3LYP functional, by up to three orders of magnitude. In the case of the M05-2X and M06-2X theories the corresponding rate constants vary from the same order of magnitude as the experimental value to an underestimate of two orders of magnitude depending on the basis set used. The rate constants predicted from the energy barriers calculated at the MP2 and PMP2 levels approach the experimental value gradually as the size and the complexity of the basis set increase. However, PMP2 val-

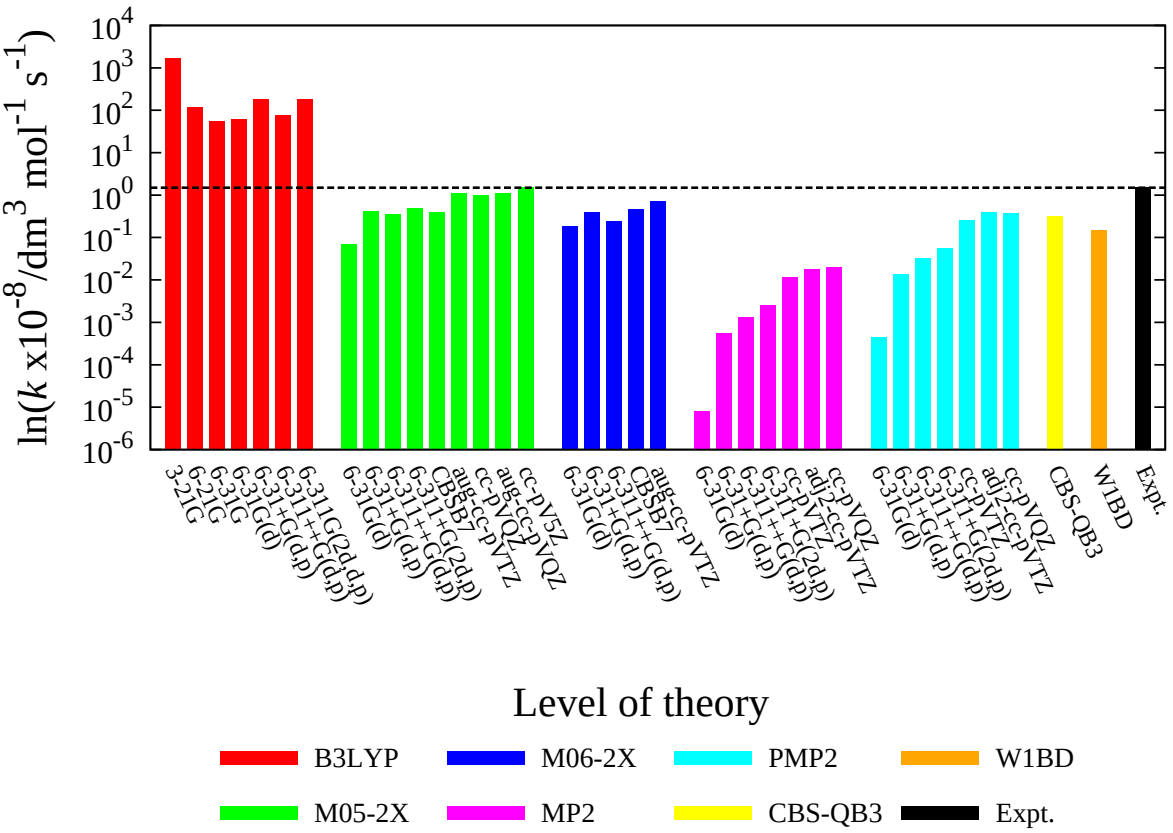

Figure 1: Rate constants of Scheme 1, calculated using Equation (3) at 298 K for various electronic structure levels of theory. Columns of the same colour correspond to the same method. For each method, the basis sets assessed are ordered from left to right in increasing order of size and complexity. The QM-calculated rate constant values at 298 K are compared with the experimental value obtained by evaluating the recommended expression given by Atkinson[10] at the same temperature. The black dashed line indicates the experimental reaction rate value so it may easily be compared to computed values.

ues only come within one order of magnitude of the experimental value (two orders for MP2), even with the use of very extended basis sets, such as aug-cc-pVTZ. The values computed with the CBS-QB3 and W1BD composite methods achieve a similar level of agreement. Our best match with the experimental value at 298 K is achieved with M05-2X/cc-pV5Z. In the following section, geometry and frequency calculations are reported using this level of theory.

Geometry and frequency calculations

The structural parameters for the reactant species C_2H_6 and ·OH, optimized using M05-2X/cc-pV5Z, are summarized in Table 2. We compare our calculated values with available equilibrium parameters estimated based on experimental data measured with spectroscopic techniques[93,94] (infrared, Raman, microwave and electronic spectroscopy in the ultraviolet and visible region) and the electron diffraction method.[93]

As may be seen in Table 2, using the M05-2X/cc-pV5Z level of theory we find bond lengths in good agreement with experimental values. For C_2H_6 our values agree best with the spectroscopic data, although for the C-C bond length our calculated value is in better agreement with the value estimated based on the electron diffraction method.

Table 2: Optimized bond lengths (r) and bond angles ($\angle$) between various atoms, calculated at the M05-2X/cc-pV5Z level of theory, for reactants C_2H_6 and ·OH in comparison with experimental values from the literature. QM=Quantum mechanics, SP=Spectroscopic techniques, ED=Diffraction Method.

	C_2H_6				·OH	
Method	$r_{\text{C-C}}$ /Å	$r_{\text{C-H}}$ /Å	$\angle_{\text{HCH}}$/°	Ref.	r/Å	Ref.
QM	1.5239	1.0864	107.76	This work	0.9683	This work
SP	1.5280	1.0877	107.31	[93]	0.9697	[94]
ED	1.5240	1.0890	106.90	[93]		

Following the geometry optimizations, frequency calculations are carried out for the reactants. The calculated vibrational frequencies, shown in Table 3, are in agreement with the harmonic frequencies observed experimentally by Hansen,[95] Miller[96] and Chase.[97] The maximum discrepancy observed is 53 cm^{-1} for the first mode for both C_2H_6 and ·OH. We note that larger differences, with a maximum of 199 cm^{-1} for C_2H_6 (fifth mode) and 218 cm^{-1} for ·OH (first mode), are observed when comparing with the fundamental frequencies reported by Shimanouchi;[98] since the calculated vibrational frequencies are obtained under the harmonic regime, such deviations are expected.

In Table 4 the geometrical parameters for the transition state structure calculated at

Table 3: Vibrational frequencies ν for the equilibrium optimized structures for the reactants C_2H_6 and ·OH at the M05-2X/cc-pV5Z level of theory and from experimental studies.

		ν/cm^{-1}				
Species	Mode	This work	Expt. Harmonic	Ref.	Expt. Fundamental	Ref.
C_2H_6	1	3096	3043	[95,96]	2954	[98]
	2	1441	1449	[95,96]	1388	[98]
	3	1021	1016	[95,96]	995	[98]
	4	303	303	[95,96]	289	[98]
	5	3095	3061	[95,96]	2896	[98]
	6	1424	1438	[95,96]	1379	[98]
	7	3142	3175	[95,96]	2969	[98]
	8	1525	1552	[95,96]	1468	[98]
	9	1235	1246	[95,96]	1190	[98]
	10	3168	3140	[95,96]	2985	[98]
	11	1528	1526	[95,96]	1469	[98]
	12	829	822	[95,96]	822	[98]
·OH	1	3788	3735	[97]	3570	[97]

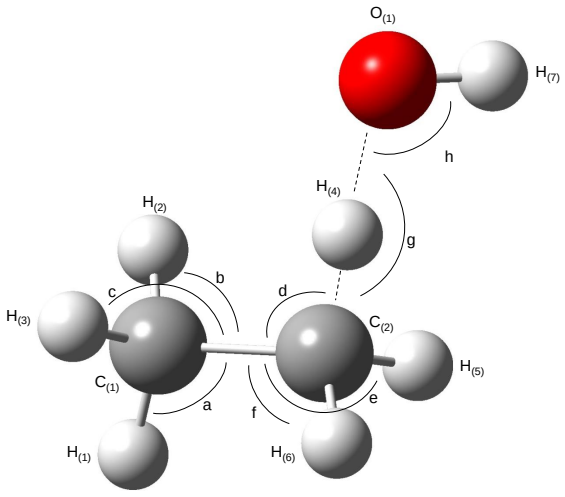

Figure 2: Optimized transition state structure at the M05-2X/cc-pV5Z level of theory. The optimized values for the bond lengths, bond angles and dihedral angles are reported in Table 4.

Table 4: Optimized structure of the transition state at the M05-2X/cc-pV5Z level of theory. The bond lengths between various atoms are represented by r, the bond angles are as specified in Figure 2, τ_1 is the $H_{(2)}$-$C_{(1)}$-$C_{(2)}$-$H_{(1)}$ dihedral angle, τ_2 is the $H_{(1)}$-$C_{(2)}$-$C_{(1)}$-$H_{(3)}$ dihedral angle, ϕ is the $H_{(4)}$-$C_{(2)}$-$C_{(1)}$-$H_{(1)}$ dihedral angle, χ_1 is the $H_{(5)}$-$C_{(2)}$-$C_{(1)}$-$H_{(4)}$ dihedral angle, χ_2 is the $H_{(4)}$-$C_{(1)}$-$C_{(2)}$-$H_{(6)}$ dihedral angle, ψ is the $O_{(1)}$-$H_{(4)}$-$C_{(2)}$-$C_{(1)}$ dihedral angle and ω is the $H_{(7)}$-$O_{(1)}$-$H_{(4)}$-$C_{(2)}$ dihedral angle.

Bond length/Å			Bond angle/°		Dihedral angle/°
$r_{C_{(1)}-C_{(2)}}$	1.5125	a	110.52	τ_1	−119.84
$r_{C_{(1)}-H_{(1)}}$	1.0885	b	111.04	τ_2	119.79
$r_{C_{(1)}-H_{(2)}}$	1.0855	c	111.05	ϕ	−179.30
$r_{C_{(1)}-H_{(3)}}$	1.0854	d	107.89	χ_1	−117.63
$r_{C_{(2)}-H_{(4)}}$	1.1587	e	113.25	χ_2	−115.73
$r_{C_{(2)}-H_{(5)}}$	1.0847	f	113.61	ψ	−95.38
$r_{C_{(1)}-H_{(6)}}$	1.0848	g	171.15	ω	−40.57
$r_{O_{(1)}-H_{(7)}}$	0.9661	h	96.66		
$r_{O_{(1)}-H_{(4)}}$	1.4380				

the M05-2X/cc-pV5Z level of theory are reported. The transition state has a staggered conformation, shown in Figure 2. The breaking bond $C_{(2)}$-$H_{(4)}$ is only 0.072 Å longer than the equivalent bond in the reactant C_2H_6 suggesting that the transition state presented here exhibits a reactant-like character. Vibrational frequency analysis of the transition state structure reveals a unique imaginary frequency (negative eigenvalue) with a value of -848 cm^{-1}.

Rate constants at different temperatures

Using the same level of theory (M05-2X/cc-pV5Z) we carry out frequency calculations for Scheme 1 at temperatures from 200 to 1250 K. To facilitate comparison with other methods, we denote these calculations as CTST/W where W refers to the Wigner transmission coefficient. Temperature-dependent experimental kinetic data are found in abundance in the literature[10,11] for this reaction. The necessary thermochemical quantities, i.e., partition functions, are recalculated at the M05-2X/cc-pV5Z level for 30 different temperature points. Our choice to employ M05-2X/cc-pV5Z is based on the close agreement achieved with the experimental rate constant at 298 K, together with the good agreement observed between

computationally and experimentally derived bond lengths and angles of the reactants..

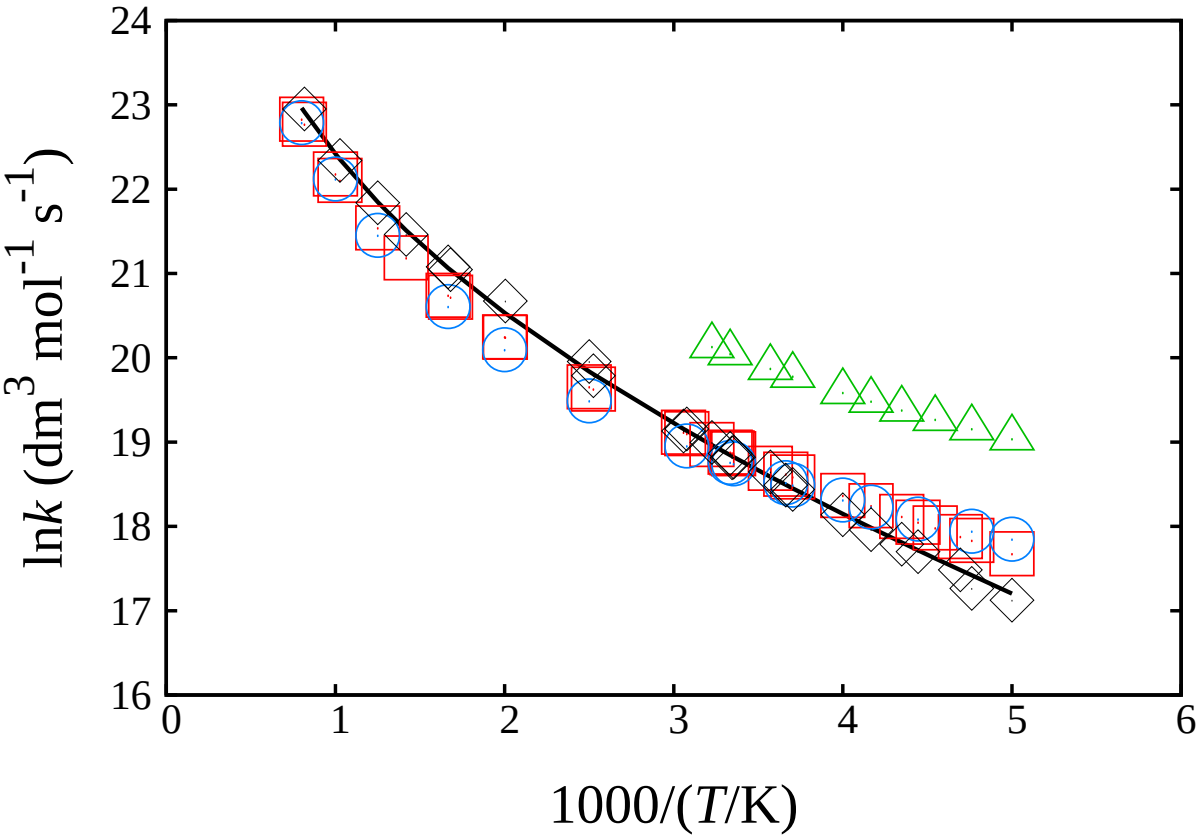

Figure 3: Rate constants of Scheme 1 as a function of inverse temperature in the range 200-1250 K. The red squares (□) correspond to the k^{IG} values calculated in this work (CTST/W), the green triangles (△) to the values computed by Hashimoto and Iwata[27] using CTST-ZCT, and the blue circles (⊙) to the values calculated by Melissas and Truhlar[19] using CVT/SCT. The black curve (—) represents the rate expression recommended by Atkinson.[10] The black diamonds (◊) indicate the experimental values[99–107] at the specific temperatures for which QM calculations are performed.

The calculated rate-constant values, obtained evaluating Equation (3) at 30 different temperatures within the range 200-1250 K, are reported in Table 5. Of the earlier computational studies that have been dedicated to this reaction, here we select and present the findings of two studies and compare them to our results. Hashimoto and Iwata[27] also employed the CTST theory but with the zero-order interpolated approximation embedded in the zero-curvature tunnelling (ZCT) method. Their calculations cover a range of low temperatures from 200 to 310 K. Melissas and Truhlar[19] employed the more advanced canonical

variational transition state theory (CVT) with small-curvature tunnelling (SCT) corrections considering a more extended temperature range from 200 K to 3000 K. Experimental data from the literature are also listed in Table 5 for comparison. The experimental values are obtained using a three-parameter expression recommended by Atkinson[10] evaluated at each of the temperatures of interest. The logarithmic values of calculated and experimental reaction rates are presented as a function of inverse temperature in an Arrhenius-like plot in Figure 3. Clear deviations from linearity are noticeable for both the experimental and the calculated values, especially for temperatures above 500 K.

Large differences are observed between our calculations and those of Hashimoto and Iwata[27] considering that both studies employ CTST. It may be seen in Table 5 that, for the temperature range considered by Hashimoto and Iwata (200-310 K), we calculate significantly lower rate-constant values with an order of magnitude difference from their values. The difference is unexpected as Hashimoto and Iwata obtained an activation energy barrier value of 8.45 kJ mol^{-1} using the CCSD(T)/aug-cc-pVDZ level of theory which is higher compared with our value of 6.65 kJ mol^{-1} at the M05-2X/cc-pV5Z level of theory (cf. Table 1). The use of frequencies and zero-point energies optimized at a lower level of theory (MP2/aug-cc-pVDZ) in their study and the use of the zero-curvature correction for tunnelling effects could be the main contributing factors to this difference. Interestingly, despite our use of the more approximate CTST, our estimated rate constants appear to be in line, if slightly overestimated with the predictions obtained by Melissas and Truhlar[19] using CVT, excepting the three lowest temperature points for which we have calculations in common, 200, 210 and 225 K. Compared with experiments, our predictions are in good agreement with the correlated values given by Atkinson[10] as well as with the individual experiments[99–107] over the entire temperature range.

In order to be able to compare quantitatively our calculations with the experimental data

Table 5: Rate constants for the kinetics of Scheme 1 obtained from different computational and experimental studies. CTST/W refers to the calculations of this work obtained at the M05-2X/cc-PV5Z level of theory using the CTST (Equation (3)) with the Wigner tunnelling factor (Equation (4)). CTST/SCT refers to the rate-constant values of Hashimoto and Iwata[27] obtained using the CTST with zero-curvature tunnelling (ZCT) correction method for the geometries and frequencies optimized at the MP2/aug-cc-pVDZ level of theory and the barrier heights obtained at the CCSD(T)/aug-cc-pVDZ level of theory. CVT/SCT refers to the rate-constant values of Melissas and Truhlar[19] obtained using the canonical-variational theory (CVT) with small-curvature tunnelling (SCT) correction method for optimized structures at the PMP2//MP2/adj2-cc-pVTZ level of theory. Atkinson's recommended expression[10] for the rate constant evaluated at the various temperatures and individual experimental values[80–87,99–107] (with the uncertainty given within the parenthesis) from the literature are also reported.

	k^{IG} $\times 10^{-8}$/dm^3 mol^{-1} s^{-1}			$k^{\mathrm{Expt.}}$ $\times 10^{-8}$/dm^3 mol^{-1} s^{-1}			
T/K	CTST/W	CTST/ZCT[27]	CVT/SCT[19]	Expt.[10]	Expt.		Ref.
200	0.474	1.855	0.564	0.296	0.273	(0.015)	[100]
210	0.556	2.090	0.620	0.367	-		
213	0.581	-	-	0.391	0.392	(0.004)	[100]
220	0.643	2.337	-	0.449	-		
225	0.690	-	0.716	0.494	0.486	(0.007)	[100]
230	0.737	2.608	-	0.542	0.531	(0.014)	[101]
240	0.838	2.897	0.825	0.646	0.632	(0.024)	[99]
250	0.945	3.210	0.897	0.762	0.753	(0.008)	[100]
270	1.180	3.896	1.072	1.030	-		
273	1.217	-	1.102	1.075	1.071	(0.026)	[101]
280	1.307	4.276	-	1.184	1.253	(0.010)	[100]
298	1.556	-	1.380	1.496	1.704	(0.117)[a]	[80–87]
299	1.569	-	-	1.512	1.482	(0.019)	[101]
300	1.583	5.095	1.403	1.530	1.560	(0.048)	[102]
310	1.732	5.540	-	1.724	1.778	(0.030)	[100]
325	1.970	-	1.704	2.041	2.086	(0.022)	[100]
327	2.002	-	-	2.086	2.035	(0.022)	[101]
355	2.498	-	-	2.773	2.764	(0.030)	[101]
396	3.342	-	-	3.991	3.920	(0.163)	[104]
400	3.432	-	2.910	4.124	4.643	(0.458)	[103]
499	6.184	-	-	8.219	9.515	(0.602)	[103]
500	6.217	-	5.336	8.269	-		
595	9.946	-	-	13.732	13.791	(1.566)	[105]
600	10.176	-	8.913	14.062	-		
705	15.875	-	-	21.975	20.957	(0.867)	[104]
800	22.639	-	20.716	30.777	30.532	(2.047)	[103]
974	39.743	-	-	50.998	50.405		[106]
1000	42.888	-	40.469	54.478	-		
1225	77.462	-	-	89.599	92.741	(14.453)	[107]
1250	82.186	-	78.890	94.056[b]	-		

[a] Average value of experimental data at 298 K reported in Table 1. The recommended value is not included.
[b] Evaluated using Atkinson's expression[10] although it is outside the recommended temperature range (180-1230 K).

of Table 5, we calculate the mean absolute percentage error (MAPE)

$$\mathrm{MAPE} = \frac{1}{N}\sum_{j=1}^{N}\left|\frac{k^{\mathrm{IG}}(T_j) - k^{\mathrm{Expt.}}(T_j)}{k^{\mathrm{Expt.}}(T_j)}\right| \times 100, \tag{5}$$

where $k^{\mathrm{IG}}(T_j)$ is a computed and $k^{\mathrm{Expt.}}(T_j)$ an experimental rate-constant value at a given temperature T_j. We also calculate the scale-dependent mean absolute error ($\mathrm{MAE_{ln}}$) for comparisons between the logarithmic values of the rate constants, given as

$$\mathrm{MAE_{ln}} = \frac{1}{N}\sum_{j=1}^{N}\left|\ln k^{\mathrm{IG}}(T_j) - \ln k^{\mathrm{Expt.}}(T_j)\right|. \tag{6}$$

Atkinson's recommended expression provides a very accurate description of the experimental kinetic data with a $\mathrm{MAE_{ln}}$ of 0.036. Henceforth comparisons are carried out with these correlated rate-constant values instead of the individual experimental data.

The overall agreement with the experimental rate constants over the whole temperature range 180-1250 K is very good with a $\mathrm{MAE_{ln}}$ of 0.213. In order to elucidate the dominant effects that impact the rate-constant calculations at different temperatures, we split the temperature range into three domains: from 200 to 299 K, from 300 to 499 K and from 500 to 1250 K; we report the $\mathrm{MAE_{ln}}$ in each domain in Table 6. In the low temperature range the QM-calculated values consistently overestimate the experimental values and the resulting value for the $\mathrm{MAE_{ln}}$ is 0.245. These deviations are most likely caused by tunnelling, which is prominent at lower temperatures. Assuming the error in these conditions arises entirely from the transmission coefficient, this would suggest that the Wigner approach overestimates the transmission coefficient in this region by a factor of 0.80 on average. In the temperature range between 300 and 499 K our computational model captures the experimental values most accurately. The calculated $\mathrm{MAE_{ln}}$ is 0.108. This agreement confirms the validity of the approximations (the use of the Wigner tunnelling correction factor and the harmonic oscillator approximation for calculating the vibrational partition functions) in this temper-

ature range. At temperatures beyond 500 K and up to 1250 K the computed rate constants systematically underestimate the experimental values, resulting in a MAE_{ln} value of 0.259. The discrepancy originates from the harmonic oscillator approximation adopted in this work which is no longer valid at such high temperatures; appropriate corrections should be considered to obtain more accurate predictions in this temperature range.[64,108] Melissas and Truhlar[19] recognised in their study the existence of hindered rotors in the transition-state structure and quantified their influence; they reported correction factors for hindered versus harmonic approximations for temperatures between 250 to 3000 K. We note that tunnelling effects contribute little, or not at all, to the error value in this area as they are almost negligible in this temperature range.

Table 6: MAPE (Equation (5)) and MAE_{ln} (Equation (6)) of QM-calculated rate-constant values with CTST/W for Scheme 1 compared with the correlated values given by Atkinson's expression[10] over temperature ranges 200-299 K, 300-499 K and 500-1250 K.

T/K	MAPE (%)	MAE_{ln}
200-1250	22.04	0.213
200-299	29.10	0.245
300-499	9.89	0.108
500-1250	22.64	0.259

Hybrid correlative models

Quantum mechanical methods may provide accurate predictions of the rate of the reaction of interest, as shown, but they are inherently difficult to validate in the absence of experimental data and they are also subject to theoretical limitations that arise from assumptions (see large deviations at high temperatures due to the harmonic approximation). Furthermore, it is not always practical to resort to such computationally demanding techniques, especially in large-scale mechanisms. On the other hand, experimental measurements may also be difficult, expensive and time-consuming. Correlative techniques, which may be very accurate and computationally fast, are often preferred.

With this in mind we consider now the combination of QM calculations with experimental kinetic data to develop correlative models of the reaction kinetics. We consider first the accuracy of commonly used Arrhenius-type[12,13] models when fitted to measured or computationally obtained rate constant data over specified temperature ranges. The estimation of reliable, statistically significant values of the Arrhenius parameters may be challenging. Large numbers of data points are usually required due to the high degree of correlation between the activation energy and the pre-exponential factor.[109,110] Here we develop a hybrid strategy for building Arrhenius-type models whose parameters are derived from both experiments and QM calculations. Through this hybrid approach we aim to improve accuracy of the model in predicting the reaction rate constant while decreasing the parametric uncertainty. The effectiveness of the proposed hybrid approaches for building reliable models using very few experimental data points is of special interest.

Methodology

The Arrhenius equation[12] has been extensively used in studies of the changes of reaction rate constants with temperature due to its simplicity and its broad applicability when narrow temperature ranges are considered. Though empirical when first formulated, the equation of Arrhenius may be related theoretically to the frequency of collisions introduced from collision theory[111,112] and the height of an energy barrier for a reaction. The combination of the two terms gives the number of successful collisions that lead to a reaction.[18]

Arrhenius-type models may be derived by defining the activation energy $E_a(T)$ at any temperature as[18]

$$\frac{\mathrm{d}\ln k}{\mathrm{d}T} = \frac{E_a(T)}{RT^2}. \tag{7}$$

If the activation energy is assumed to be equal to a value $\tilde{E}_a$ independent of temperature, so that

$$E_a(T) = \tilde{E}_a, \tag{8}$$

after integration Equation (7) reduces to the well-known equation

$$k_1 = A_1 \exp\left(-\frac{\tilde{E}_a}{RT}\right), \tag{9}$$

or, in logarithmic form, to

$$\ln k_1 = \ln A_1 - \frac{\tilde{E}_a}{RT}, \tag{10}$$

where A_1 is the so-called pre-exponential factor. Subscript "1" is used hereafter to refer to quantities obtained when assuming the activation energy is temperature-independent. Experimentally measured or predicted rate-constant values may be used to determine A_1 and $\tilde{E}_a$ in a very straightforward manner. The assumption of a temperature-independent activation energy leads to a linear dependency of $\ln k_1$ on $1/T$ which is well known to be an oversimplification (cf. the data and results in the previous section). Alternatively, if a linear dependence is used for $E_a(T)$, the following expression is often postulated:[113]

$$E_a(T) = E_a^\star + mRT, \tag{11}$$

where $E_a^\star$ and m are temperature-independent parameters. In this case the rate constant is obtained from Equation (7) as

$$k_2 = A_2 T^m \exp\left(-\frac{E_a^\star}{RT}\right), \tag{12}$$

where an additional temperature dependence appears in the pre-exponential factor through parameter m and the pre-exponential factor A_2 is temperature-independent as before. In logarithmic form the expression is given as

$$\ln k_2 = \ln A_2 + m \ln T - \frac{E_a^\star}{RT}. \tag{13}$$

This expression is usually referred to as the generalized Arrhenius (GA) equation.[13] Subscript

"2" hereafter refers to quantities obtained when assuming the activation energy is linearly dependent on temperature (Equation (11)). For a given reaction, parameter $E_a^\star$ should not typically be expected to be the same as the activation energy $\tilde{E}_a$ appearing in the original Arrhenius equation.

The GA expression is usually applied when data show significant deviations from linearity - either due to large experimental uncertainty, or, more often, due to extended temperature ranges being considered. For cases when the kinetic data fail to comply to the linearity dictated by the Arrhenius equation, satisfactory results are found when analysing those data in terms of the GA expression.[10,114,115] It is important, however, to note that even in the case of highly accurate experimental kinetic data, there might exist several widely different parameter sets that may fit almost equally well the data when using Equation (12); in other words, the inherent uncertainty of estimating the GA parameters is significant.

In the context of our work it is useful to relate the activation energies resulting from the Arrhenius and GA models to quantities computed via electronic structure (QM) methods. At a given temperature the Gibbs free energy of a reaction may be written in terms of its enthalpic and entropic contributions as

$$\Delta^\ddagger \underline{G}^{\circ,\mathrm{IG}}(T) = \Delta^\ddagger \underline{H}^{\circ,\mathrm{IG}}(T) - T\Delta^\ddagger \underline{S}^{\circ,\mathrm{IG}}(T), \tag{14}$$

where $\Delta^\ddagger \underline{H}^{\circ,\mathrm{IG}}(T)$ is the ideal-gas enthalpy of activation and $\Delta^\ddagger \underline{S}^{\circ,\mathrm{IG}}(T)$ is the ideal-gas entropy of activation. Substituting Equation (14) in Equation (1) results in

$$k^{\mathrm{IG}} = \kappa \frac{k_\mathrm{B} T}{h} \prod_{i=\mathrm{A,B,AB}^\ddagger} \left(\frac{RT}{p^\circ}\right)^{-\nu_i} \exp\left(\frac{\Delta^\ddagger \underline{S}^{\circ,\mathrm{IG}}(T)}{R}\right) \exp\left(-\frac{\Delta^\ddagger \underline{H}^{\circ,\mathrm{IG}}(T)}{RT}\right), \tag{15}$$

which may be written in a more concise form as

$$k^{\mathrm{IG}} = C(T) \exp\left(-\frac{\Delta^\ddagger \underline{H}^{\circ,\mathrm{IG}}(T)}{RT}\right), \tag{16}$$

or, in logarithmic form, as

$$\ln k^{\mathrm{IG}} = \ln C(T) - \frac{\Delta^{\ddagger}\underline{H}^{\circ,\mathrm{IG}}(T)}{RT}, \tag{17}$$

where the pre-exponential temperature-dependent term takes the form

$$C(T) = \kappa \frac{k_{\mathrm{B}}T}{h} \prod_{i=\mathrm{A,B,AB}^{\ddagger}} \left(\frac{RT}{p^{\circ}}\right)^{-\nu_i} \exp\left(\frac{\Delta^{\ddagger}\underline{S}^{\circ,\mathrm{IG}}(T)}{R}\right), \tag{18}$$

or

$$\ln C(T) = \ln\left(\kappa \frac{k_{\mathrm{B}}T}{h}\right) - \sum_{i=\mathrm{A,B,AB}^{\ddagger}} \nu_i \ln\left(\frac{RT}{p^{\circ}}\right) + \frac{\Delta^{\ddagger}\underline{S}^{\circ,\mathrm{IG}}(T)}{R}. \tag{19}$$

Equating Equations (13) and (17) and differentiating them with respect to temperature, neglecting the temperature dependence of entropy results in an expression that links parameters $E_a^{\star}$ and m to the activation enthalpy:[18]

$$E_a^{\star} = \Delta^{\ddagger}\underline{H}^{\circ,\mathrm{IG}}(T) + (1 - m - \sum_{i=\mathrm{A,B,AB}^{\ddagger}} \nu_i)RT. \tag{20}$$

The activation enthalpy term is related to the electronic energy barrier, $\Delta^{\ddagger}\underline{E}^{\mathrm{el,IG}}$, obtained from QM calculations as

$$\Delta^{\ddagger}\underline{H}^{\circ,\mathrm{IG}}(T) = \Delta^{\ddagger}\underline{E}^{\mathrm{el,IG}} + \Delta^{\ddagger}\underline{E}^{\mathrm{therm}}(T) + \sum_{i=\mathrm{A,B,AB}^{\ddagger}} \nu_i RT, \tag{21}$$

where $\Delta^{\ddagger}\underline{E}^{\mathrm{therm}}(T)$ is a correction term for the internal thermal activation energy accounting for the effects of molecular translation, rotation and vibration. Substituting Equation (21) in Equation (20) results in

$$E_a^{\star} = \Delta^{\ddagger}\underline{E}^{\mathrm{el,IG}} + \Delta^{\ddagger}\underline{E}^{\mathrm{therm}}(T) + (1 - m)RT, \tag{22}$$

which may be further inserted into Equation (13) to give

$$k_2 = A_2 T^m \exp\left(-\frac{\Delta^\ddagger \underline{E}^{\mathrm{el,IG}} + \Delta^\ddagger \underline{E}^{\mathrm{therm}}(T)}{RT} - (1-m)\right), \tag{23}$$

or

$$\ln k_2 = \ln A_2 + m \ln T - \frac{\Delta^\ddagger \underline{E}^{\mathrm{el,IG}} + \Delta^\ddagger \underline{E}^{\mathrm{therm}}(T)}{RT} - (1-m). \tag{24}$$

In Equation (24) quantities $\Delta^\ddagger \underline{E}^{\mathrm{el,IG}}$ and $\Delta^\ddagger \underline{E}^{\mathrm{therm}}$ are obtained from QM calculations and the remaining parameters A_2 and m may be obtained by fitting to available experimental reaction rate data. We refer to this as a hybrid approach since we employ both experimental and computed data to estimate the reaction rate constant.

Arrhenius-type hybrid models

In this section, different combinations of experimental and computational data are used, sometimes for the entire temperature range studied and sometimes for just a few temperature points, with the aim to derive the parameters of Equations (10), (13) and (24) such that they reproduce the known experimental reaction rate data and such that the values of the derived parameters are statistically significant and specifically their confidence intervals are as small as possible. In Table 7 the different models developed in this work are presented. For each model the equation on which the model is based is given. Whether experimental data or QM-calculated data or a combination of both are used for fitting a model's parameters is indicated by descriptors such as 'Expt.', which refers to the use of experimental reaction rate constants, and 'QM', which refers to QM-calculated rate constants with CTST/W or activation energy values at the M05-2X/cc-pV5Z level of theory obtained in this work. Within the parenthesis following the descriptors the temperature range over which data are taken is indicated (either the entire temperature range from 200 to 1250 K or a specific number of temperature points, in which case the points are explicitly written).

We first develop model "Arrhenius", which refers to the use of the Arrhenius equa-

Table 7: Data sets used to estimate the parameters of the various Arrhenius-type models developed in this study for the kinetics of Scheme 1. Parameters A_1 and $\tilde{E}_a$ refer to Equation (10). Parameters A_2, m and $E_a^\star$ refer to Equation (13). Descriptor "Expt." refers to experimental reaction rate data. Descriptor "QM" refers to QM-calculated reaction rate data obtained with CTST/W or activation energy values at the M05-2X/cc-pV5Z level of theory. Within the parenthesis following the descriptors , the range or the specific point(s) of temperature at which data are fitted is given. Regarding the experimental data, for the entire temperature range the equation of Atkinson[10] is used while for the specific temperature points the experimental values of Talukdar et al.[101] are used. HM=Hybrid Model.

Model	Equation No.	A_1	m	$\tilde{E}_a$
Arrhenius	(10)	Expt.(200-1250)	-	Expt.(200-1250)
Model	**Equation No.**	A_2	m	$E_a^\star$
GA	(13)	Expt.(200-1250)	Expt.(200-1250)	Expt.(200-1250)
GA^{QM}	(13)	QM(200-1250)	QM(200-1250)	QM(200-1250)
HM A	(24)	Expt.(200-1250)	Expt.(200-1250)	Expt.(200-1250), QM(298)[a]
GA_{4T}	(13)	Expt.(273, 299, 327, 355)	Expt.(273, 299, 327, 355)	Expt.(273, 299, 327, 355)
HM A_{4T}	(24)	Expt.(273, 299, 327, 355)	Expt.(273, 299, 327, 355)	Expt.(273, 299, 327, 355), QM(298)[a]

[a] Calculated using Equation (22) at 298 K.

tion (Equation (10)), and model GA, which refers to the generalized-Arrhenius equation (Equation (13)), by fitting both of them to the experimental reaction rate data of Atkinson over the temperature range from 200 to 1250 K.[10] Model GA^{QM} refers to the use of the generalized-Arrhenius equation (Equation (13)) fitted to QM-calculated reaction rate constants as computed using CTST/W. It should be noted that model GA^{QM} is purely predictive as it is based entirely on QM calculations. A hybrid strategy is then considered in the case of model HM A, which refers to a hybrid model based on the understanding that parameter $E_a^\star$ has the largest impact on the calculation of reaction kinetics as it is directly linked to the activation barrier height of the reaction. In this model $E_a^\star$ is given by Equation (22), with quantities $\Delta^\ddagger \underline{E}^{\mathrm{el,IG}}$ and $\Delta^\ddagger \underline{E}^{\mathrm{therm}}$ obtained from QM calculations at the M05-2X/cc-pV5Z level of theory, and parameters A_2 and m obtained by fitting to experimental reaction rate data in the range from 200 to 1250 K. In developing model HM A we take full advantage of the information provided by available experimental reaction rate data while performing only the minimum number of QM calculations possible: a fixed value for the thermal correction activation energy term at 298 K is assumed instead of recalculating this quantity at each individual temperature assessed. This assumption significantly reduces the time required to develop the hybrid model.

Models GA_{4T} and HM A_{4T} are of particular interest here. In these, instead of using the entire temperature range, only four temperature points, taken over a narrow temperature range, are considered. By reducing the number of data points, we significantly reduce the amount of information that is needed to compute the reaction rate constants. This reduction in data increases the intrinsic uncertainty of the parameters in the models but it is a relevant scenario in many reactions for which only a few experimental data points are available or for which only a few QM computations may be performed. In the development of models GA_{4T} and HM A_{4T}, m and A_2 are determined by fitting to experimental reaction rate constants at 273, 299, 327 and 355 K; in addition, in model HM A_{4T}, $E_a^\star$ is obtained from Equation (22) by carrying out QM calculations at the M05-2X/cc-pV5Z level of theory to obtain $\Delta^\ddagger \underline{E}^{\mathrm{el,IG}}$ and $\Delta^\ddagger \underline{E}^{\mathrm{therm}}$, as in model HM A. Rate constants at the four temperature points (273, 299, 327, 355 K), are those reported by Talukdar et al.[101] We choose this set of values as they are sufficiently spread above and below the 298 K temperature and are evenly distributed.

Results

Performance of the models

A model's accuracy in capturing a certain data set is often not enough to render the model successful for application; the statistical significance of the parameters constituting the model is also important. In Table 8 the parameters for the various models and their 95% confidence intervals are listed. The corresponding MAE_{ln} values calculated by comparison with the experimental reaction rate data of Atkinson[10] using the entire temperature range (200-1250 K) are also reported in Table 8. In Figure 4 the various models developed in this study are presented and compared with the experimental reaction rate data fitted by Atkinson's expression.[10]

Inspecting Table 8 and Figure 4, it may be seen that all the models perform well and capture the experimental reaction rate data. The GA model (Figure 4a) performs best, fitting the experimental reaction rate data over the entire temperature range studied with a MAE_{ln}

Table 8: Comparison of parameters and their 95% confidence intervals (CI) for the various Arrhenius-type models developed for the kinetics of Scheme 1. Parameters A_1 and A_2 are given in dm^3 mol^{-1} s^{-1} and parameters $\tilde{E}_a$ and $E_a^\star$ are given in kJ mol^{-1}. The MAE$_{\ln}$ (Equation (5)) is also reported, comparing with the experimental reaction rate data for Scheme 1, as shown in Table 5 for the range 200-1250 K. HM=Hybrid Model.

Model	A_1	95% CI	m	95% CI	$\tilde{E}_a$	95% CI	MAE$_{\ln}$
Arrhenius	1.54×10^{10}	1.21×10^{10}-1.96×10^{10}	-	-	11.07	10.43-11.70	0.220
Model	A_2	95% CI	m	95% CI	$E_a^\star$	95% CI	MAE$_{\ln}$
GA	9.00×10^{3}	8.92×10^{3}-9.08×10^{3}	2.00	1.99-2.01	4.15	4.14-4.16	0.002
GA$^{\mathrm{QM}}$	1.04×10^{4}	0.00-3.50×10^{4}	1.91	1.58-2.24	3.00	1.83-4.17	0.195
HM A	5.20×10^{5}	2.98×10^{5}-7.41×10^{5}	1.39	1.32-1.45	5.43[a]	5.28-5.58	0.069
GA$_{4\mathrm{T}}$	1.08×10^{4}	0.00-2.33×10^{6}	1.97	0.00-33.69	4.19	0.00-85.97	0.021
HM A$_{4\mathrm{T}}$	2.45×10^{6}	0.00-8.97×10^{6}	1.15	0.75-1.54	6.02[a]	5.05-7.00	0.118

[a] Calculated using Equation (20) at 298 K.

value of 0.002. The negligible error value of this approach is not surprising as the model exploits the entire set of experimental reaction rate data available and its three-parameter form allows for temperature effects to be taken into account. Use of the Arrhenius model leads to the largest error (MAE$_{\ln}$=0.220) due to the lack of temperature dependence in the pre-exponential factor which, given the broad temperature range studied in this work, is an unrealistic assumption. It is interesting to consider model GA$^{\mathrm{QM}}$ now, which leads to a MAE$_{\ln}$ of 0.195. As shown in Figure 4b, this model results in larger deviations from the experimental reaction rate data at low (overestimating) and high (underestimating) temperature regions while it performs better in the intermediate temperature range. However, acknowledging that model GA$^{\mathrm{QM}}$ is purely predictive, the agreement with experimental reaction rate data for the entire temperature range from 200 to 1250 K may be considered good. Model GA$^{\mathrm{QM}}$ was developed using exclusively QM-calculated reaction rate data, hence when comparison is made with those QM-calculated values for the entire temperature range (200 to 1250 K) (cf. Table 5) the corresponding error value, denoted as MAE$_{\ln}^{\mathrm{QM}}$, is low (0.090). Hybrid model HM A is in good agreement with the experimental rate constants; the calculated MAE$_{\ln}$ is 0.069. In contrast to the QM-based model GA$^{\mathrm{QM}}$, in which no experimental information is used, we find that using experimental reaction rate data to fit two of the three

parameters (m and A_2) lowers the corresponding error value considerably and enhances the model's range of applicability as shown in Figure 4b. The fact that hybrid model HM A performs better than the classical Arrhenius model, with a $\mathrm{MAE_{ln}}$ value much lower than 0.220 (cf. Table 8), is also encouraging.

The models using the reduced data[101] developed in this study (GM $\mathrm{A_{4T}}$ and HM $\mathrm{A_{4T}}$) may be considered especially successful; they lead to comparatively low $\mathrm{MAE_{ln}}$ values across the entire temperature range even though only four experimental data points are needed over a narrow range. In model $\mathrm{GA_{4T}}$ the level of accuracy achieved is very good (cf. Figure 4c). The experimental reaction rate data of Atkinson[10] are reproduced with a $\mathrm{MAE_{ln}}$ value of 0.021 (the second lowest error of this study). For hybrid model HM $\mathrm{A_{4T}}$ the agreement achieved with experimental reaction rate data is also very good, with a $\mathrm{MAE_{ln}}$ value of 0.118, a much lower value than those of the $\mathrm{GA^{QM}}$ model and the classical Arrhenius model. These results highlight the benefits of combining experimental and QM-calculated information in the development of these models.

Model parameters and statistical significance

The classical Arrhenius model relies on two parameters (A_1 and $\tilde{E}_a$) compared with all the other models considered in this work, which contains three parameters (A_2, m and $E_a^\star$). As a result, distinctly different values are obtained for parameters A_1 and A_2, and $\tilde{E}_a$ and $E_a^\star$ (cf. Table 8) and thus, comparisons regarding parameter values are made only between the three-parameter models. Nevertheless, it is interesting to note that although there is a difference of six orders of magnitude between parameters A_1 and A_2, this has a relatively small impact on the predicted rate constants indicating the smaller influence that the pre-exponential factor has on the value of the rate constant. Parameters A_1 and A_2 are inherently difficult to estimate, as is perceivable from the large confidence intervals obtained for these parameters in all the models derived here, even in cases where an extensive set of reaction rate data (experimental or QM-calculated) is used. Conversely, parameter $\tilde{E}_a$ in

(a)

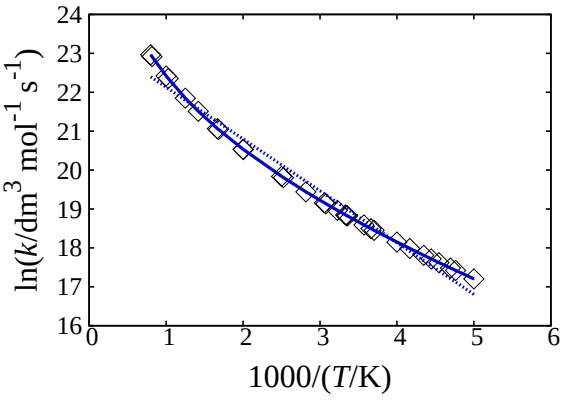

(b)

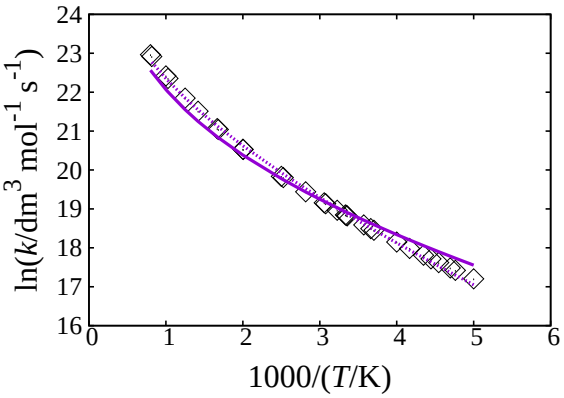

(c)

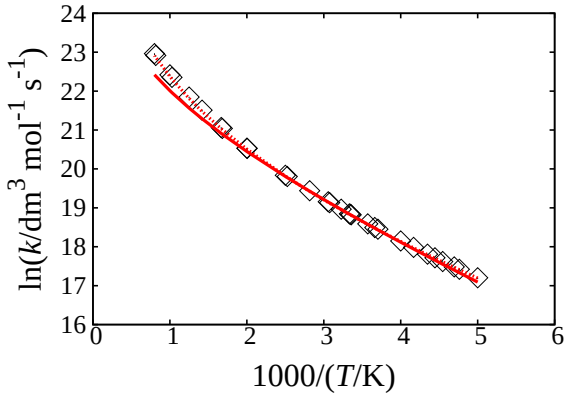

Figure 4: Arrhenius plots of the various models developed in this work compared with experimental reaction rate data reported by Atkinson[10] for Scheme 1 over a temperature range from 200 to 1250 K, as shown in Table 5, illustrated here by black diamonds (◊). (a) GA model (—) and Arrhenius model (· · ·). (b) GA^{QM} model (—) and HM A model (· · ·). (c) GA_{4T} model (—) and HM A_{4T} model (· · ·).

the Arrhenius model is well characterized with a comparatively narrow confidence interval, lying in a range of ± 0.63 kJ mol^{-1} of the central value.

Of the three-parameter models considered, the GA model is the one resulting in the tightest 95% confidence intervals for its three parameters. This observation is in line with the expectation of obtaining statistically reliable parameters when an abundance of experimental data is available. In this model, the values we obtain for parameters m and $E_a^\star$, with narrow 95% confidence intervals of ± 0.01 of the central value in each case, are identical to the values reported by Atkinson in his recommended reaction rate expression.[10] Also, evaluating Equation (11) at 298 K, using the GA model parameter values, results in a value of 9.11 kJ mol^{-1} for the $E_a(298)$ parameter, which is comparable with the value of 11.07 kJ mol^{-1} found for $\tilde{E}_a$ in the classical Arrhenius model. Interestingly, the values estimated for all three parameters A_2, m and $E_a^\star$ of the GA model are included within the 95% confidence intervals of models GA$^{\mathrm{QM}}$ and GA$_{4\mathrm{T}}$. They are not in the 95% confidence intervals of either of the hybrid models (HM A or HM A$_{4\mathrm{T}}$), with the exception of A_2 in the GA model which is included in the 95% confidence interval of A_2 in the HM A$_{4\mathrm{T}}$ model.

Reducing the number of experimental values used for the fitting of the reaction rate data drastically increases the uncertainty in the estimated parameters A_2, m and $E_a^\star$ and as a consequence, the corresponding 95% confidence intervals broaden. This is clearly noticeable in models GA$_{4\mathrm{T}}$ and HM A$_{4\mathrm{T}}$ and more so in model GA$_{4\mathrm{T}}$ because only experimental sources of information are used in developing this model and so it effectively has one more fitted parameters than model HM A$_{4\mathrm{T}}$. The values for the fitted parameters for model GA$_{4\mathrm{T}}$ are very similar to the parameter values found for the GA model and lie just outside the 95% confidence intervals. However, the 95% confidence intervals of all three parameters A_2, m and $E_a^\star$ of model GA$_{4\mathrm{T}}$ are larger by a factor of 10^4 (or more) than the 95% confidence intervals of model GA. In summary, the large value of the 95% confidence intervals of model GA$_{4\mathrm{T}}$ suggests that this model consists of statistically unreliable parameters. By comparison, in model HM A$_{4\mathrm{T}}$, reducing the number of experimental data points has a smaller impact

on the 95% confidence intervals of the parameters. We obtain the confidence interval of parameter $E_a^\star$ in the hybrid models by evaluation of Equation (20) for the low and high bound values of the 95% confidence interval of parameter m. The use of the QM-calculated activation energy values in parameter $E_a^\star$ together with the experimental data selected results in tighter confidence intervals. This is the key advantage of our proposition of hybrid models.

Discussion

Based on the preceding analysis, a number of recommendations may be made for the use of each of the models proposed in this work considering their suitability in terms of the level of accuracy that may be needed to capture the reaction rate data, the amount of available reaction rate data (experimental or QM-calculated) and the intrinsic uncertainty carried by the estimated parameters.

When an abundance of experimentally measured reaction rate data is available, speaking strictly in terms of accuracy, the empirical model GA leads to the best agreement with the experimental data. Our proposed hybrid model HM A appears as an appealing alternative, capturing the gas-phase kinetics of Scheme 1 very well, in particular far better than the empirical Arrhenius model, which is conventionally used in many kinetic studies. As part of the hybrid strategy to build model HM A, performing one extra QM calculation and obtaining information relevant to parameter $E_a^\star$ has the advantage of reducing the $\mathrm{MAE_{ln}}$ of the rate-constant value by 0.150 compared with the conventional Arrhenius model's $\mathrm{MAE_{ln}}$ value. In addition, more reliable estimates for parameters A_2, m and $E_a^\star$ with narrower 95% confidence intervals are obtained; this is a key advantage of the hybrid model. The importance of the hybrid strategy is particularly highlighted when few data are available. In the scenario of considering only four experimental reaction data points at different temperatures, again speaking strictly in terms of accuracy, the $\mathrm{GA_{4T}}$ model provides the best agreement with the experimental data; however, its estimated parameters in this case are, to a very large extent, statistically meaningless. By comparison, our hybrid model HM $\mathrm{A_{4T}}$, seems quite robust,

with one of the two parameters estimated (m) especially well-defined, when fitted to four temperature points (273, 299, 327, 355 K), and very good overall agreement (MAE_{ln}=0.118) achieved, including extrapolation to a large range of temperatures (180-1250 K).

Conclusions

The effect of temperature on the kinetics of a hydrogen abstraction reaction has been studied computationally. We have identified the best quantum-mechanical (QM) method for describing accurately the kinetics of this reaction and we have further developed a novel hybrid approach to build better correlative models by combining QM calculations with experimental data.

For the calculation of the activation energy barrier of the reaction, a thorough screening of various levels of theory was carried out. Accounting for spin-contamination effects was found to improve the accuracy of the calculated activation barrier for the reaction; thus, unrestricted and spin-projected methods were used. Our calculations indicated that B3LYP fails to produce reasonable results, giving negative values for the activation barrier. The use of M05-2X and M06-2X results in positive activation barriers, in agreement with experiments, with lower values for more complex basis sets. Predicted activation barriers lie between 6.65 and 15.26 kJ mol^{-1} for M05-2X and between 7.91 and 13.27 kJ mol^{-1} for M06-2X for different basis sets. A similar pattern was observed for MP2 and PMP2, which gave gradually decreasing values of the activation barrier for increasingly complex basis sets. The lowest overall activation barrier was calculated at the M05-2X/cc-pV5Z level. For each of the levels of theory tested, the corresponding rate constants were calculated at 298 K. Conventional transition state theory, with the Wigner[42] correction factor accounting for tunnelling effects, was used. The M05-2X/cc-pV5Z level of theory gave a rate constant value of 1.556 $\times 10^8$ dm^3 mol^{-1} s^{-1} which is in remarkably good agreement with the experimental value 1.496$\times 10^8$ dm^3 mol^{-1} s^{-1} obtained using a three-parameter Generalized Arrhenius-type formula[10] reported

by Atkinson.[10] Optimized structures and vibrational frequencies for the reactants at 298 K, calculated at the same level of theory, also agreed well with experimental measurements.

The temperature dependence of the reaction rate constant was studied in a broad temperature range between 200 and 1250 K. Good agreement with experimental reaction rate constants, obtained by evaluation of Atkinson's expression,[10] was achieved at the M05-2X/cc-pV5Z level. An overall MAE_{ln} of 0.213 was found comparing with experimental data for the whole temperature range studied. A MAE_{ln} value of 0.108 was found comparing with the experimental rate constants over an intermediate temperature range (300-499 K), in which the validity of our assumptions concerning the tunnelling effect and the harmonic approximation is guaranteed. Our findings are also in line with the results of Melissas and Truhlar[19] who used variational transition state theory to calculate the reaction rate constants of the same reaction. The good agreement observed with their calculations indicates that CTST may be used to describe the kinetics of the reaction of interest when combined with a highly accurate computational method, such as the M05-2X/cc-pV5Z level of theory, without the need for the more advanced variational transition state theory.

New hybrid correlative models, based on a generalized Arrhenius form, have been proposed to predict reaction rates combining QM-calculated reaction rate data and activation energy values with experimental reaction rate data. We find that these hybrid models offer the best balance between model accuracy and precision of the estimated parameters (narrow confidence intervals). Particularly, hybrid model HM A_{4T}, where only four experimental reaction rate data points at four different temperatures are considered and in which one QM calculation is performed at 298 K to obtain information pertinent to parameter $E_a^\star$, proved a good alternative to the empirical GA_{4T} model. The MAE_{ln} value for the HM A_{4T} model was 0.118, compared with the corresponding value of 0.021 for the GA_{4T} model. Moreover, two of the three parameters (m and $E_a^\star$) included in the HM A_{4T} model were found to be well characterized with tight confidence intervals (approximately ± 0.4 and ± 0.98 kJ mol^{-1} of the central values, respectively) compared with the ill-defined parameters found for the

GA_{4T} model. Due to its pre-exponential nature parameter A_2 is intrinsically difficult to characterize accurately in either model.

Overall the hybrid models proposed in this work constitute a useful predictive approach that may be easily extended to other reactions. These hybrid models offer the advantage of incorporating valuable information from experiments in their parameters, while achieving good reliability (statistical significance). They require less experimental effort to develop than fully empirical models and they may prove a particularly useful tool when studying reactions for which a limited number of experimental reaction rate data exist.

Acknowledgement

Financial support from Syngenta as well as access to computational resources and support from the High Performance Computing Cluster at Imperial College London are gratefully acknowledged.

Data statement

Data underlying this article may be accessed on Zenodo at 10.5281/zenodo.61379 and used under the Creative Commons Attribution licence.

References

(1) Gardiner, Jr., W. C., Ed. *Gas-Phase Combustion Chemistry*, 2nd ed.; Springer-Verlag: New York, 2000; p 543.

(2) Barker, J. R., Ed. *Progress and Problems in Atmospheric Chemistry*; World Scientific: Singapore, 1995; p 956.

(3) Seinfeld, J. H. Global Atmospheric Chemistry of Reactive Hydrocarbons. In *Reactive Hydrocarbons in the Atmosphere*; Hewitt, C. N., Ed.; Academic Press: San Diego, 1999; Chapter 8, pp 293–319.

(4) Stanbury, D. M. Reactivity of Inorganic Radicals in Aqueous Solution. In *Physical Inorganic Chemistry*; Bakac, A., Ed.; John Wiley & Sons, Inc.: Hoboken, NJ, USA, 2010; Chapter 9, pp 395–427.

(5) Wilson, Jr., W. E. A Critical Review of the Gas-Phase Reaction Kinetics of the Hydroxyl Radical. *J. Phys. Chem. Ref. Data* **1972**, *1*, 535–574.

(6) Atkinson, R. Kinetics and Mechanisms of the Gas-Phase Reactions of the Hydroxyl Radical with Organic Compounds under Atmospheric Conditions. *Chem. Rev.* **1986**, *86*, 69–201.

(7) Atkinson, R. Kinetics and Mechanisms of the Gas-Phase Reactions of the Hydroxyl Radical with Organic Compounds. *J. Phys. Chem. Ref. Data, Monograph 1,* **1989**, 1–246.

(8) Atkinson, R. Gas-phase Tropospheric Chemistry of Organic Compounds. *J. Phys. Chem. Ref. Data, Monograph 2,* **1994**, 1–216.

(9) Atkinson, R. Gas-phase Tropospheric Chemistry of Volatile Organic Compounds: 1. Alkanes and Alkenes. *J. Phys. Chem. Ref. Data* **1997**, *26*, 215–290.

(10) Atkinson, R. Kinetics of the Gas-Phase Reactions of OH Radicals with Alkanes and Cycloalkanes. *Atmos. Chem. Phys.* **2003**, *3*, 2233–2307.

(11) Wilson, Jr., E. W.; Hamilton, W. A.; Kennington, H. R.; Evans, III, B.; Scott, N. W.; DeMore, W. B. Measurement and Estimation of Rate Constants for the Reactions of Hydroxyl Radical with Several Alkanes and Cycloalkanes. *J. Phys. Chem. A* **2006**, *110*, 3593–3604.

(12) Arrhenius, S. A. Über die Reaktionsgeschwindigkeit bei der Inversion von Rohrzucker durch Säuren. *Z. Phys. Chem.* **1889**, *4*, 226–248.

(13) Kooij, D. M. Über die Zersetzung des gasförmigen Phosphorwasserstoffs. *Z. Phys. Chem.* **1893**, *12*, 155–161.

(14) Smith, I. W. M. The Temperature-Dependence of Elementary Reaction Rates: Beyond Arrhenius. *Chem. Soc. Rev.* **2008**, *37*, 812–826.

(15) Temelso, B.; Sherrill, C. D.; Merkle, R. C.; Freitas, Jr., R. A. High-level Ab Initio Studies of Hydrogen Abstraction from Prototype Hydrocarbon Systems. *J. Phys. Chem. A* **2006**, *110*, 11160–11173.

(16) Zhao, Y.; González-García, N.; Truhlar, D. G. Benchmark Database of Barrier Heights for Heavy Atom Transfer, Nucleophilic Substitution, Association, and Unimolecular Reactions and Its Use to Test Theoretical Methods. *J. Phys. Chem. A* **2005**, *109*, 2012–2018.

(17) Zheng, J.; Zhao, Y.; Truhlar, D. G. Representative Benchmark Suites for Barrier Heights of Diverse Reaction Types and Assessment of Electronic Structure Methods for Thermochemical Kinetics. *J. Chem.Theory Comput.* **2007**, *3*, 569–582.

(18) Atkins, P.; de Paula, J. *Atkins' Physical Chemistry*, 8th ed.; Oxford University Press: Oxford, 2006; p 1053.

(19) Melissas, V. S.; Truhlar, D. C. Interpolated Variational Transition-State Theory and Semiclassical Tunneling Calculations of the Rate Constant of the Reaction OH+C2H6 at 200-3000 K. *J. Phys. Chem.* **1994**, *98*, 875–886.

(20) Martell, J. M.; Mehta, A.; Pacey, P. D.; Boyd, R. J. Properties of Transition Species in the Reaction of Hydroxyl with Ethane from Ab Initio Calculations and Fits to Experimental Data. *J. Phys. Chem.* **1995**, *99*, 8661–8668.

(21) Sekušak, S.; Güsten, H.; Sabljić, A. An Ab Initio Investigation on Transition States

and Reactivity of Chloroethane with OH Radical. *J. Chem. Phys.* **1995**, *102*, 7504–7518.

(22) Jursic, B. S. Density Functional Theory Study of Radical Hydrogen Abstraction with Hydrogen and Hydroxyl Radicals. *Chem. Phys. Lett.* **1996**, *256*, 603–608.

(23) Sekušak, S.; Liedl, K. R.; Rode, B. M.; Sabljić, A. Reaction-Path Dynamics of Hydroxyl Radical Reactions with Ethane and Haloethanes. *J. Phys. Chem. A* **1997**, *101*, 4245–4253.

(24) Sekušak, S.; Cory, M. G.; Bartlett, R. J.; Sabljić, A. Dual-Level Direct Dynamics of the Hydroxyl Radical Reaction with Ethane and Haloethanes: Toward a General Reaction Parameter Method. *J. Phys. Chem. A* **1999**, *103*, 11394–11405.

(25) García-Cruz, I.; Ruiz-Santoyo, M. E.; Alvarez-Idaboy, J. R.; Vivier-Bunge, A. Ab-Initio Study of Initial Atmospheric Oxidation Reactions of C3 and C4 Alkanes. *J. Comput. Chem.* **1999**, *20*, 845–856.

(26) Chuang, Y. Y.; Coitiño, E. L.; Truhlar, D. G. How Should We Calculate Transition State Geometries for Radical Reactions? The Effect of Spin Contamination on the Prediction of Geometries for Open-Shell Saddle Points. *J. Phys. Chem. A* **2000**, *104*, 446–450.

(27) Hashimoto, T.; Iwata, S. Theoretical Study on the Weakly-Bound Complexes in the Reactions of Hydroxyl Radical with Saturated Hydrocarbons (Methane, Ethane, and Propane). *J. Phys. Chem. A* **2002**, *106*, 2652–2658.

(28) Krasnoperov, L. N.; Michael, J. V. Shock Tube Studies Using a Novel Multipass Absorption Cell: Rate Constant Results for OH+H2 and OH+C2H6. *J. Phys. Chem. A* **2004**, *108*, 5643–5648.

(29) Bravo-Pérez, G.; Alvarez-Idaboy, J. R.; Galano-Jimenéz, A.; Cruz-Torres, A. Quantum Chemical and Conventional TST Calculations of Rate Constants for the OH+Alkane Reaction. *Chem. Phys.* **2005**, *310*, 213–223.

(30) Hu, X. P.; Wang, B. X.; Gao, Y.; Yang, B. Theoretical Investigation of Mechanism for the Gas-Phase Reaction of OH Radical and Ethane. *J. At. Mol. Sci.* **2011**, *2*, 225–233.

(31) Curtiss, L. A.; Raghavachari, K.; Trucks, G. W.; Pople, J. A. Gaussian-2 theory for molecular energies of first-and second-row compounds. *J. Chem. Phys.* **1991**, *94*, 7221–7230.

(32) Pople, J. A.; Head-Gordon, M.; Raghavachari, K. Quadratic configuration interaction. A general technique for determining electron correlation energies. *J. Chem. Phys.* **1987**, *87*, 5968–5975.

(33) Paldus, J.; Čížek, J.; Shavitt, I. Correlation Problems in Atomic and Molecular Systems. IV. Extended Coupled-Pair Many-Electron Theory and Its Application to the BH3 Molecule. *Phys. Rev. A* **1972**, *5*, 50–67.

(34) Schaefer, III, H. F. Interaction Potentials I: Atom-Molecule Potentials. In *Atom-Molecule Collision Theory: A Guide for the Experimentalist*; Bernstein, R. B., Ed.; Plenum Press: New York, 1979; Chapter 2, pp 45–78.

(35) Johnson, B. G.; Gill, P. M. W.; Pople, J. A. A Rotationally Invariant Procedure for Density Functional Calculations. *Chem. Phys. Lett.* **1994**, *220*, 377–384.

(36) Zhang, Y.; Yang, W. A Challenge for Density Functionals: Self-Interaction Error Increases for Systems with a Noninteger Number of Electrons. *J. Chem. Phys.* **1998**, *109*, 2604–2608.

(37) Patchkovskii, S.; Ziegler, T. Improving "Difficult" Reaction Barriers with Self-

Interaction Corrected Density Functional Theory. *J. Chem. Phys.* **2002**, *116*, 7806–7813.

(38) Lynch, B. J.; Truhlar, D. G. How Well Can Hybrid Density Functional Methods Predict Transition State Geometries and Barrier Heights? *J. Phys. Chem. A* **2001**, *105*, 2936–2941.

(39) Sumathi, R.; Green, Jr., W. H. A Priori Rate Constants for Kinetic Modeling. *Theor. Chem. Acc.* **2002**, *108*, 187–213.

(40) Eyring, H. The Activated Complex in Chemical Reactions. *J. Chem. Phys.* **1935**, *3*, 107–115.

(41) Evans, M. G.; Polanyi, M. Some Applications of the Transition State Method to the Calculation of Reaction Velocities, Especially in Solution. *Trans. Faraday Soc.* **1935**, *31*, 875–894.

(42) Wigner, E. Calculation of the Rate of Elementary Association Reactions. *J. Chem. Phys.* **1937**, *5*, 720–725.

(43) Frisch, M. J.; Trucks, G. W.; Schlegel, H. B.; Scuseria, G. E.; Robb, M. A.; Cheeseman, J. R.; Scalmani, G.; Barone, V.; Mennucci, B.; Petersson, G. A.; Nakatsuji, H.; Caricato, M.; Li, X.; Hratchian, H. P.; Izmaylov, A. F.; Bloino, J.; Zheng, G.; Sonnenberg, J. L.; Hada, M.; Ehara, M.; Toyora, K.; Fukuda, R.; Hasegawa, J.; Ishida, M.; Nakajima, T.; Honda, Y.; Kitao, O.; Nakai, H.; Vreven, T.; Montgomery, J. A.; Peralta, Jr., J. E.; Ogliaro, F.; Bearpark, M.; Heyd, J. J.; Brothers, E.; Kudin, K. N.; Staroverov, V. N.; Kobayashi, R.; Normand, J.; Raghavachari, K.; Rendell, A.; Burant, J. C.; Iyengar, S. S.; Tomasi, J.; Cossi, M.; Rega, N.; Millam, J. M.; Klene, M.; Knox, J. E.; Cross, J. B.; Bakken, V.; Adamo, C.; Jaramillo, J.; Gomperts, R.; Stratmann, R. E.; Yazyev, O.; Austin, A. J.; Cammi, R.; Pomelli, C.; Ochterski, J. W.;

Martin, R. L.; Morokuma, K.; Zakrzewski, V. G.; Voth, G. A.; Salvador, P.; Dannenberg, J. J.; Dapprich, S.; Daniels, A. D.; Farkas, O.; Foresman, J. B.; Ortiz, J. V.; Cioslowski, J.; Fox, D. J. Gaussian 09 Revision C.01. 2009.

(44) Becke, A. D. Density Functional Thermochemistry. III. The Role of Exact Exchange. *J. Chem. Phys.* **1993**, *98*, 5648–5652.

(45) Lee, C.; Yang, W.; Parr, R. G. Development of the Colle-Salvetti Correlation Energy Formula into a Functional of the Electron Density. *Phys. Rev. B* **1988**, *37*, 785–789.

(46) Vosko, S. H.; Wilk, L.; Nusair, M. Accurate Spin-Dependent Electron Liquid Correlation Energies for Local Spin Density Calculations: A Critical Analysis. *Can. J. Phys.* **1980**, *58*, 1200–1211.

(47) Stephens, P.; Devlin, F. J.; Chabalowski, C. F.; Frisch, M. J. Ab Initio Calculation of Vibrational Absorption and Circular Dichroism Spectra Using Density Functional Force Fields. *J. Phys. Chem.* **1994**, *98*, 11623–11627.

(48) Zhao, Y.; Schultz, N. E.; Truhlar, D. G. Design of Density Functionals by Combining the Method of Constraint Satisfaction with Parametrization for Thermochemistry, Thermochemical Kinetics, and Noncovalent Interactions. *J. Chem. Theory Comput.* **2006**, *2*, 364–382.

(49) Zhao, Y.; Truhlar, D. G. The M06 Suite of Density Functionals for Main Group Thermochemistry, Thermochemical Kinetics, Noncovalent Interactions, Excited States, and Transition Elements: Two New Functionals and Systematic Testing of Four M06-Class Functionals and 12 Other Function. *Theor. Chem. Acc.* **2008**, *120*, 215–241.

(50) Head-Gordon, M.; Pople, J. A.; Frisch, M. J. MP2 Energy Evaluation by Direct Methods. *Chem. Phys. Lett.* **1988**, *153*, 503–506.

(51) Löwdin, P. O. Quantum Theory of Many-Particle Systems. III. Extension of the Hartree-Fock Scheme to Include Degenerate Systems and Correlation Effects. *Phys. Rev.* **1955**, *97*, 1509–1520.

(52) Schlegel, H. B. Potential Energy Curves Using Unrestricted Møller-Plesset Perturbation Ttheory with Spin Annihilation. *J. Chem. Phys.* **1986**, *84*, 4530–4534.

(53) Montgomery, Jr., J. A.; Frisch, M. J.; Ochterski, J. W.; Petersson, G. A. A Complete Basis Set Model Chemistry. VI. Use of Density Functional Geometries and Frequencies. *J. Chem. Phys.* **1999**, *110*, 2822–2827.

(54) Montgomery, Jr., J. A.; Frisch, M. J.; Ochterski, J. W.; Petersson, G. A. A Complete Basis Set Model Chemistry. VII. Use of the Minimum Population Localization Method. *J. Chem. Phys.* **2000**, *112*, 6532–6542.

(55) Barnes, E. C.; Petersson, G. A.; Montgomery, J. A.; Frisch, M. J.; Martin, J. M. L. Unrestricted Coupled Cluster and Brueckner Doubles Variations of W1 Theory. *J. Chem. Theory Comput.* **2009**, *5*, 2687–2693.

(56) Martin, J. M. L.; de Oliveira, G. Towards Standard Methods for Benchmark Quality Ab Initio Thermochemistry - W1 and W2 Theory. *J. Chem. Phys.* **1999**, *111*, 1843–1856.

(57) Scott, A. P.; Radom, L. Harmonic Vibrational Frequencies: An Evaluation of Hartree-Fock, Møller-Plesset, Quadratic Configuration Interaction, Density Functional Theory, and Semiempirical Scale Factors. *J. Phys. Chem.* **1996**, *100*, 16502–16513.

(58) Wong, M. W.; Radom, L. Radical Addition To Alkenes: An Assessment of Theoretical Procedures. *J. Phys. Chem.* **1995**, *99*, 8582–8588.

(59) Koopmans, T. Über die Zuordnung von Wellenfunktionen und Eigenwerten zu den Einzelnen Elektronen Eines Atoms. *Physica* **1934**, *1*, 104–113.

(60) Knowles, P. J.; Handy, N. C. Projected Unrestricted Møller-Plesset Second-Order Energies. *J. Chem. Phys.* **1988**, *88*, 6991.

(61) Kobayashi, Y.; Kamiya, M.; Hirao, K. The Hydrogen Abstraction Reactions: A Multireference Møller-Plesset Perturbation (MRMP) Theory Study. *Chem. Phys. Lett.* **2000**, *319*, 695–700.

(62) Young, D. C. Spin contamination. In *Computational chemistry: A Practical Guide for Applying Techniques to Real World Problems*; Wiley-Interscience: New York; Chicester, 2001; Chapter 27, pp 227–230.

(63) Wynne-Jones, W. F. K.; Eyring, H. The Absolute Rate of Reactions in Condensed Phases. *J. Chem. Phys.* **1935**, *3*, 492–502.

(64) McQuarrie, D. A. *Statistical Mechanics*; University Science Books: Sausalito, California; Great Britain, 2000; p 641.

(65) Skodje, R. T.; Truhlar, D. G.; Garrett, B. C. A General Small-Curvature Approximation for Transition State-Theory Transmission Coefficients. *J. Phys. Chem.* **1981**, *85*, 3019–3023.

(66) Eckart, C. The Penetration of a Potential Barrier by Electrons. *Phys. Rev.* **1930**, *35*, 1303–1309.

(67) Johnston, H.; Rapp, D. Large Tunnelling Corrections in Chemical Reaction Rates. *J. Am. Chem. Soc.* **1961**, *83*, 1–9.

(68) Vandeputte, A. G.; Sabbe, M. K.; Reyniers, M. F.; Van Speybroeck, V.; Waroquier, M.; Marin, G. B. Theoretical Study of the Thermodynamics and Kinetics of Hydrogen Abstractions from Hydrocarbons. *J. Phys. Chem. A* **2007**, *111*, 11771–11786.

(69) Vandeputte, A. G.; Sabbe, M. K.; Reyniers, M. F.; Marin, G. B. Kinetics of α Hydrogen Abstractions from Thiols, Sulfides and Thiocarbonyl Compounds. *Phys. Chem. Chem. Phys.* **2012**, *14*, 12773–12793.

(70) Lu, D. H.; Truong, T. N.; Melissas, V. S.; Lynch, G. C.; Liu, Y. P.; Garrett, B. C.; Steckler, R.; Issacson, A. D.; Rai, S. N.; Hancock, G. C.; Lauderdale, J. G.; Joseph, T.; Truhlar, D. G. POLYRATE 4: A New Version of a Computer Program for the Calculation of Chemical Reaction Rates for Polyatomics. *Comput. Phys. Commun.* **1992**, *71*, 235–262.

(71) Liu, Y. P.; Lynch, G. C.; Truong, T. N.; Lu, D. H.; Truhlar, D. C.; Garrett, B. C. Molecular Modeling of the Kinetic Isotope Effect for the [1,5] Sigmatropic Rearrangement of cis-1,3-Pentadiene. *J. Am. Chem. Soc.* **1993**, *115*, 2408–2415.

(72) Fernandez-Ramos, A.; Truhlar, D. G. Improved algorithm for corner-cutting tunneling calculations. *Journal of Chemical Physics* **2001**, *114*, 1491–1496.

(73) Jursic, B. S. The Hydrogen Abstraction from Ethane with a Hydrogen Radical as Examined with Ab Initio and Density Functional Theory Methods. *J. Mol. Struct.-Theochem* **1998**, *428*, 49–54.

(74) Jursic, B. S. Ab Initio and Density Function Theory Computational Studies of the CH4+H to CH3+H2 Reaction. *J. Mol. Struct.-Theochem* **1998**, *430*, 17–22.

(75) Zhao, Y.; Truhlar, D. G. Density Functionals with Broad Applicability in Chemistry. *Acc. Chem. Res.* **2008**, *41*, 157–167.

(76) Cramer, C. J. *Essentials of Computational Chemistry: Theories and Models*, 2nd ed.; Wiley: Chichester, 2004; p 596.

(77) Chandra, A. K.; Uchimaru, T. An ab Initio Investigation of the Reactions of 1,1- and 1,2-Dichloroethane with Hydroxyl Radical. *J. Phys. Chem. A* **1999**, *103*, 10874–10883.

(78) Jursic, B. S. Computing transition state structures with density functional theory methods. In *Recent Developments and Applications of Modern Density Functional Theory*; Seminario, J. M., Ed.; Theoretical and Computational Chemistry, Vol. 4; Elsevier: The Netherlands, 1996; pp 709–741.

(79) Hall, M. L.; Goldfeld, D. A.; Bochevarov, A. D.; Friesner, R. A. Localized Orbital Corrections for the Calculations of Barrier Heights in Density Functional Theory. *J. Chem. Theory Comput.* **2009**, *5*, 2996–3009.

(80) Greiner, N. R. Hydroxyl Radical Kinetics by Kinetic Spectroscopy. VI. Reactions with Alkanes in the Range 300-500 K. *J. Chem. Phys.* **1970**, *53*, 1070–1076.

(81) Leu, M. T. Rate Constant for the Reaction HO2+NO to OH+NO2. *J. Chem. Phys.* **1979**, *70*, 1662–1666.

(82) Jeong, K. M.; Hsu, K. J.; Jeffries, J. B.; Kaufman, F. Kinetics of the Reactions of OH with C2H6, CH3CCl3, CH2ClCHCl2, CH2ClCClF2 and CH2FCF3. *J. Phys. Chem.* **1984**, *88*, 1222–1226.

(83) Schiffman, A.; Nelson, Jr., D. D.; Robinson, M. S.; Nesbittt, D. J. High-Resolution Infrared Flash Kinetic Spectroscopy of OH Radicals. *J. Phys. Chem.* **1991**, *95*, 2629–2636.

(84) Dóbé, S.; Turányi, T.; Bérces, T.; Márta, F. The Kinetics of Hydroxyl Radical Reactions with Cyclopentane and Cyclobutane. Proceedings of the Indian Academy of Sciences - Chemical Sciences. India, 1991; pp 499–503.

(85) Dóbé, S.; Turányi, T.; Bérces, T. Rate Constants of the Reactions of OH Radicals with Cyclopentane and Cyclobutane. *Int. J. Chem. Kinet.* **1992**, *24*, 191–198.

(86) Sharkey, P.; Smith, I. W. M. Kinetics of Elementary Reactions at Low Temperatures:

Rate Constants for the Reactions of OH with HCl (138-298 K), CH4 (178-298 K) and C2H6 (138-298 K). *J Chem. Soc. Faraday Trans.* **1993**, *89*, 631–638.

(87) Finlayson-Pitts, B. J.; Hernandez, S. K.; Berko, H. N. A New Dark Source of the Gaseous Hydroxyl Radical for Relative Rate Measurements. *J. Phys. Chem.* **1993**, *97*, 1172–1177.

(88) Ditchfield, R.; Hehre, W. J.; Pople, J. A. Self-Consistent Molecular-Orbital Methods. IX. An Extended Gaussian-Type Basis for Molecular-Orbital Studies of Organic Molecules. *J. Chem. Phys.* **1971**, *54*, 724–728.

(89) Dunning, Jr., T. H. Gaussian Basis Sets for Use in Correlated Molecular Calculations. I. The Atoms Boron Through Neon and Hydrogen. *J. Chem. Phys.* **1989**, *90*, 1007–1023.

(90) Dunning, Jr., T. H.; Peterson, K. A.; Woon, D. E. Basis sets: correlation consistent. In *Encyclopedia of Computational Chemistry*; Schleyer, P. v. R., Ed.; John Wiley & Sons, Ltd, 2002; pp 88–115.

(91) Zhao, Y.; Lynch, B. J.; Truhlar, D. . Multi-Coefficient Extrapolated Density Functional Theory for Thermochemistry and Thermochemical Kinetics. *Phys. chem. chem. phys.* **2005**, *7*, 43–52.

(92) Zhao, Y.; Truhlar, D. G. Exploring the Limit of Accuracy of the Global Hybrid Meta Density Functional for Main-Group Thermochemistry, Kinetics, and Noncovalent Interactions. *J. Chem. Theory Comput.* **2008**, *4*, 1849–1868.

(93) Duncan, J. L.; McKean, D. C.; Bruce, A. J. Infrared Spectroscopic Studies of Partially Deuterated Ethanes and the r0, rz, and re Structures. *J. Mol. Spectrosc.* **1979**, *74*, 361–374.

(94) Haynes, W. M. *CRC Handbook of Chemistry and Physics*, 96th ed.; 2015; p 2677.

(95) Hansen, G. E.; Dennison, D. M. The Potential Constants of Ethane. *J. Chem. Phys.* **1952**, *20*, 313–326.

(96) Miller, K. J.; Ganda-Kesuma, F. S. An Empirical Rule Relating Fundamental to Harmonic Frequencies. *J. Mol. Spectrosc.* **1991**, *145*, 429–447.

(97) Chase, Jr., M. W. NIST-JANAF Thermochemical Tables, Fourth Edition, Part 1, Al-Co. *J. Phys. Chem. Ref. Data, Monograph 9,* **1998**, 1963.

(98) *Tables of Molecular Vibrational Frequencies. Consolidated Volume I - Takehiko Shimanouchi*; NSRDS-NBS 39: U.S., 1972; p 167.

(99) Smith, C. A.; Molina, L. T.; Lamb, J. J.; Molina, M. J. Kinetics of the Reaction of OH with Pernitric and Nitric Acids. *Int. J. Chem. Kinet.* **1984**, *16*, 41–55.

(100) Clarke, J. S.; Kroll, J. H.; Donahue, N. M.; Anderson, J. G. Testing Frontier Orbital Control: Kinetics of OH with Ethane, Propane, and Cyclopropane from 180 to 360 K. *J. Phys. Chem. A* **1998**, *102*, 9847–9857.

(101) Talukdar, R. K.; Mellouki, A.; Gierczak, T.; Barone, S.; Chiang, S. Y.; Ravishankara, A. R. Kinetics of the Reactions of OH with Alkanes. *Int. J. Chem. Kinet.* **1994**, *26*, 973–990.

(102) Donahue, N. M.; Anderson, J. G.; Demerjian, K. L. New Rate Constants for Ten OH Alkane Reactions from 300 to 400 K: An Assessment of Accuracy. *J. Phys. Chem. A* **1998**, *102*, 3121–3126.

(103) Tully, F. P.; Ravishankara, A. R.; Carr, K. Kinetic Study of the Reactions of the Hydroxyl Radical with Ethane and Propane. *Int. J. Chem. Kinet.* **1983**, *15*, 1111–1118.

(104) Tully, F. P.; Droege, A. T.; Koszykowski, M. L.; Melius, C. F. Hydrogen-Atom Abstraction from Alkanes by OH. 2. Ethane. *J. Phys. Chem.* **1986**, *90*, 691–698.

(105) Baulch, D. L.; Craven, R. J. B.; Din, M.; Drysdale, D. D.; Grant, S.; Richardson, D. J.; Walker, A.; Watling, G. Rates of Hydroxy Radical Reactions with Methane, Ethane and Propane over the Temperature Range 403-696 K. *J. Chem. Soc., Faraday Trans. 1* **1983**, *79*, 689–698.

(106) Koffend, J. B.; Cohen, N. Shock Tube Study of OH Reactions with Linear Hydrocarbons near 1100 K. *Int. J. Chem. Kinet.* **1996**, *28*, 79–87.

(107) Bott, J. F.; Cohen, N. A Shock Tube Study of the Reaction of Methyl Radicals with Hydroxyl Radicals. *Int. J. Chem. Kinet.* **1991**, *23*, 1017–1033.

(108) Hill, T. L. *An Introduction to Statistical Thermodynamics*; Dover Publications: New York, 1986.

(109) Asprey, S. P.; Macchietto, S. Statistical Tools for Optimal Dynamic Model Building. *Computers & Chemical Engineering* **2000**, *24*, 1261–1267.

(110) Macchietto, S. *Dynamic Model Development: Methods, Theory and Applications*; Elsevier Science: Burlington, 2003; p 267.

(111) Trautz, M. Das Gesetz der Reaktionsgeschwindigkeit und der Gleichgewichte in Gasen. Bestätigung der Additivität von Cv-3/2R. Neue Bestimmung der Integrationskonstanten und der Molekül durchmesser. *Z. Anorgan. Chem.* **1916**, *96*, 1–28.

(112) Lewis, W. XLI. Studies in Catalusis. Part IX. The Calculation in Absolute Measure of Velocity Constants and Equilibrium Constants in Gaseous Systems. *J. Chem. Soc., Trans.* **1918**, *113*, 471–492.

(113) Laidler, K. J. *Chemical Kinetics*, 3rd ed.; Harper and Row: New York; London, 1987.

(114) Gardiner, Jr., W. C. Temperature Dependence of Bimolecular Gas Reaction Rates. *Acc. Chem. Res.* **1977**, *10*, 326–331.

(115) Whytock, D. A.; Lee, J. H.; Michael, J. V.; Payne, W. A.; Stief, L. J. Absolute Rate of the Reaction of Cl(2P) with Methane from 200-500 K. *J. Chem. Phys.* **1977**, *66*, 2690–2695.